Lecture Notes in Electrical Engineering 389

Jiadong Sun
Jingnan Liu
Shiwei Fan
Feixue Wang
Editors

China Satellite Navigation Conference (CSNC) 2016 Proceedings: Volume II

Springer

Lecture Notes in Electrical Engineering

Volume 389

About this Series

"Lecture Notes in Electrical Engineering (LNEE)" is a book series which reports the latest research and developments in Electrical Engineering, namely:

- Communication, Networks, and Information Theory
- Computer Engineering
- Signal, Image, Speech and Information Processing
- Circuits and Systems
- Bioengineering

LNEE publishes authored monographs and contributed volumes which present cutting edge research information as well as new perspectives on classical fields, while maintaining Springer's high standards of academic excellence. Also considered for publication are lecture materials, proceedings, and other related materials of exceptionally high quality and interest. The subject matter should be original and timely, reporting the latest research and developments in all areas of electrical engineering.

The audience for the books in LNEE consists of advanced level students, researchers, and industry professionals working at the forefront of their fields. Much like Springer's other Lecture Notes series, LNEE will be distributed through Springer's print and electronic publishing channels.

More information about this series at http://www.springer.com/series/7818

Jiadong Sun · Jingnan Liu
Shiwei Fan · Feixue Wang
Editors

China Satellite Navigation Conference (CSNC) 2016 Proceedings: Volume II

Springer

Editors
Jiadong Sun
Chinese Academy of Sciences
China Aerospace Science and Technology Corporation
Beijing
China

Jingnan Liu
Wuhan University
Wuhan
China

Shiwei Fan
China Satellite Navigation Office
Beijing
China

Feixue Wang
National University of Defense Technology
Changsha
China

ISSN 1876-1100 ISSN 1876-1119 (electronic)
Lecture Notes in Electrical Engineering
ISBN 978-981-10-0936-5 ISBN 978-981-10-0937-2 (eBook)
DOI 10.1007/978-981-10-0937-2

Library of Congress Control Number: 2016937343

Printed on acid-free paper

This Springer imprint is published by Springer Nature
The registered company is Springer Science+Business Media Singapore Pte Ltd.

Preface

BeiDou Navigation Satellite System (BDS) is China's global navigation satellite system which has been developed independently. BDS is similar in principle to global positioning system (GPS) and compatible with other global satellite navigation systems (GNSS) worldwide. The BDS will provide highly reliable and precise positioning, navigation and timing (PNT) services as well as short-message communication for all users under all-weather, all-time, and worldwide conditions.

China Satellite Navigation Conference (CSNC) is an open platform for academic exchanges in the field of satellite navigation. It aims to encourage technological innovation, accelerate GNSS engineering, and boost the development of the satellite navigation industry in China and in the world.

The 7th China Satellite Navigation Conference (CSNC2016) is held during May 18–20, 2016, Changsha, China. The theme of CSNC2016 is Smart Sensing, Smart Perception, including technical seminars, academic exchanges, forums, exhibitions, and lectures. The main topics are as follows:

S1 BDS/GNSS Application Technology
S2 Navigation and Location-Based Services
S3 Satellite Navigation Signals
S4 Satellite Orbit and Clock Offset Determination
S5 BDS/GNSS Precise Positioning Technology
S6 Atomic Clock and Time-frequency Technology
S7 BDS/GNSS Augmentation Systems and Technology
S8 BDS/GNSS Test and Assessment Technology
S9 BDS/GNSS User Terminal Technology
S10 Multi-sensor Fusion Navigation
S11 PNT System and Emerging Navigation Technology
S12 Standardization, Intellectual Properties, Policies, and Regulations

The proceedings (Lecture Notes in Electrical Engineering) have 176 papers in ten topics of the conference, which were selected through a strict peer-review process from 440 papers presented at CSNC2016. In addition, another 193 papers

were selected as the electronic proceedings of CSNC2016, which are also indexed by "China Proceedings of Conferences Full-text Database (CPCD)" of CNKI and Wan Fang Data.

We thank the contribution of each author and extend our gratitude to 237 referees and 48 session chairmen who are listed as members of editorial board. The assistance of CNSC2016's organizing committees and the Springer editorial office is highly appreciated.

The 7th China Satellite Navigation Conference (CSNC 2016) Committees

Scientific Committee

Chairman
Jiadong Sun, China Aerospace Science and Technology Corporation

Vice-Chairman
Rongjun Shen, China
Jisheng Li, China
Qisheng Sui, China
Changfei Yang, China
Zuhong Li, China Academy of Space Technology
Shusen Tan, Beijing Satellite Navigation Center, China

Executive Chairman
Jingnan Liu, Wuhan University
Yuanxi Yang, China National Administration of GNSS and Applications
Shiwei Fan, China

Committee Members (By Surnames Stroke Order)
Xiancheng Ding, China Electronics Technology Group Corporation
Qingjun Bu, China
Liheng Wang, China Aerospace Science and Technology Corporation
Yuzhu Wang, Shanghai Institute of Optics and Fine Mechanics, Chinese Academy of Sciences
Guoxiang Ai, National Astronomical Observatories, Chinese Academy of Sciences
Shuhua Ye, Shanghai Astronomical Observatories, Chinese Academy of Sciences
Zhaowen Zhuang, National University of Defense Technology
Qifeng Xu, PLA Information Engineering University
Houze Xu, Institute of Geodesy and Geophysics, Chinese Academy of Sciences
Guirong Min, China Academy of Space Technology

Xixiang Zhang, China Electronics Technology Group Corporation
Lvqian Zhang, China Aerospace Science and Technology Corporation
Junyong Chen, National Administration of Surveying, Mapping and Geoinformation
Benyao Fan, China Academy of Space Technology
Dongjin Luo, China
Guohong Xia, China Aerospace Science and Industry Corporation
Chong Cao, China Research Institute of Radio Wave Propagation (CETC 22)
Faren Qi, China Academy of Space Technology
Sili Liang, China Aerospace Science and Technology Corporation
Shancheng Tu, China Academy of Space Technology
Rongsheng Su, China
Zhipeng Tong, China Electronics Technology Group Corporation
Ziqing Wei, Xi'an Institute of Surveying and Mapping

Organizing Committee

Secretary General
Haitao Wu, Navigation Headquarters, Chinese Academy of Sciences

Vice Secretary General
Wenhai Jiao, China Satellite Navigation Office Engineering Center
Jianjun Wu, National University of Defense Technology
Weina Hao, Navigation Headquarters, Chinese Academy of Sciences

Committee Members (By Surnames Stroke Order)
Qun Ding, The 20th Research Institute of China Electronics Technology Group Corporation
Miao Yu, China Academy of Space Technology
Li Wang, International Cooperation Research Center China Satellite Navigation Engineering Office
Ying Liu, China Satellite Navigation Office Engineering Center
Shuhua Zhang, National University of Defense Technology, Changsha
Xiuwan Chen, Peking University
Xiangan Zhao, China Defense Science and Technology Information Center
Ouyang Guangzhou, Academy of Opto-electronics, Chinese Academy of Sciences
Gang Hu, Beijing Unicore Communications, Inc.
Min Shui, National Remote Sensing Centre of China
Zhong Dou, National Time Service Center, Chinese Academy of Sciences

Editorial Board

Topic S5: BDS/GNSS Precise Positioning Technology
BDS/GNSS Precise Positioning Technology
Qile Zhao, Wuhan University
Jianwen Li, Information Engineering University
Song shuLi, Shanghai Astronomical Observatory, Chinese Academy of Sciences
Yanming Feng, Queensland University of Technology, Brisbane, Australia

Topic S6: Atomic Clock and Time-frequency Technology
Lianshan Gao, The 203th Research Institute of China Aerospace Science and Industry Corporation
Chunhao Han, Beijing Satellite Navigation Center
Xiaohui Li, National Time Service Center, Chinese Academy of Sciences
Nikolay Demidov, VCH Corporation, Russia

Topic S7: BDS/GNSS Augmentation Systems and Technology
Junlin Zhang, OLinkStar Co., Ltd., China
Jinping Chen, Beijing Satellite Navigation Center
Rui Li, Beihang University
Shaojun Feng, Imperial College London

Topic S8: BDS/GNSS Test and Assessment Technology
Jun Yang, National University of Defense Technology
Xiaolin Jia, Xi'an Institute of Surveying and Mapping
Wenxian Yu, Shanghai Jiao Tong University
Yang Gao, University of Calgary, Canada

Topic S9: BDS/GNSS User Terminal Technology
Haibo He, Beijing Satellite Navigation Center
Baowang Lian, Northwestern Polytechnical University
Hong Li, Tsinghua University
Yong Li, University of New South Wales, Australia

Topic S10: Multi-sensor Fusion Navigation
Zhongliang Deng, Beijing University of Posts and Telecommunications
Hong Yuan, Academy of Opto-electronics, Chinese Academy of Sciences
Yongbin Zhou, National University of Defense Technology
Jinling Wang, University of New South Wales, Australia

Topic S11: PNT System and Emerging Navigation Technology
Mingquan Lu, Tsinghua University
Wei Wang, The 20th Research Institute of China Electronics Technology Group Corporation
Yin Xu, Academy of Opto-electronics, Chinese Academy of Sciences
Xiangzhen Li, Chungnam National University, Korea

Contents

Part I
Satellite Navigation Signals

The Application of Fountain Code in Satellite Navigation System

Qiao Liu, Wenjing Zhang, Yong Wang and Hui Li

Abstract The research on satellite navigation signal is one of the most essential topics in satellite navigation system. The enhancement of the signal will undoubtedly improve the service quality of navigation system. Dealing with this problem, applying latest emerging coding schemes have been proved to be efficient. Therefore, we analyze the application of fountain code into satellite navigation system in this paper. To achieve better transmission, we first propose a modified encoding algorithm to reduce the minimized transmission packets cost. Further, by introducing Low-Earth orbit satellite, we concatenate digital fountain code with traditional channel code. By doing so, we can optimize the utilization of fountain code in satellite channels. Finally, simulation results are conducted to valid our theoretical analysis.

Keywords Fountain code · Satellite navigation system · Concatenated code

1 Introduction

The satellite navigation signals are the direct factors to affect the quality of navigation service. However, the navigation signals suffer a bad signal-to-noise condition due to the satellite communication channel properties. Therefore, the instability of navigation signals is always the bottleneck for the navigation service. Abundant of solutions have been explored to improve the navigation signal transmitting. Among them, applying error correction code, including LDPC, Turbo, and RS code, has been proved to be an efficient way. Following such approach, this paper applies the latest emerging close Shannon limit code, i.e., fountain code, into the satellite navigation system.

The idea of fountain code is first proposed over binary erasure channel in 1998, and this idea is realized into practice by LT code in [4] and Raptor code in [5].

Q. Liu (✉) · W. Zhang · Y. Wang · H. Li
ISN, School of Cyber Engineering, Xidian University, Xi'an, China
e-mail: qiao.liu@uwaterloo.ca; windachilles@gmail.com

J. Sun et al. (eds.), *China Satellite Navigation Conference (CSNC) 2016 Proceedings: Volume II*, Lecture Notes in Electrical Engineering 389,
DOI 10.1007/978-981-10-0937-2_1

Following these two well-known fountain codes, the research has been divided into two directions. One is the code improvement and another is the code application. For the fountain code improvement, the degree distribution attracts most attentions [6]. Besides degree distribution, the encoding and decoding algorithms have also been analyzed, see [1]. For the application, the usage of fountain code has been extended into more channel models rather than binary erasure channel, like Block fading channels [2] and AWGN channels [3]. The fountain code also witnesses its application in different networks, like [7, 8]. In particular, the authors in [8] apply the LT code into satellite communication with an enhanced decoding algorithm. We hold an identical motivation with [8] to apply the fountain code into satellite communication, however, with a different approach.

Besides the error correction code, another technique is also attracted enough attention to be a promising method to improve satellite navigation, namely Low-Earth orbit (LEo) satellite. The LEo satellites have a better transmission channel than the Medium-Earth orbit (MEo) satellite for its low distance to the Earth surface, where the MEo contains most navigation satellites. Utilizing LEo satellite in communication becomes a hot topic in the last few years, however the recent connection between LEo satellites and navigation only lies in the locating of LEo satellites by the GPS. Thus, a novel scheme is desired to improve navigation signal with help of LEo satellites.

Following previous discussed motivations, we apply the fountain code into satellite navigation system. Rather than a naive transplanting, the encoding algorithm is modified to reduce the redundancy cost. Further, by involving the LEo satellites, the fountain code is concatenated with error correction code. These two approaches are also the main contributions of this work.

2 Fountain Code

2.1 Overview of the Fountain Code

The fountain code is name after a metaphorical sense in which considers the transmission as a process of filling water into a bucket. During the transmission, the transmitter encodes and sends its messages like a fountain, and the receiver, comparing to a bucket, will continually receive the water until correct decoding. Thus, one round of information transmitting is completed.

The encoder unit of fountain code is packet. It means that the encoder in the transmitter will first divides the source file into fixed length packets, and then encodes each packet. The receiver will continually collect these encoded packets and make an attempt to recovering all of them.

In practical, the number of the received packets is a little larger than the encoded packets number but uncertain. Therefor the rate of the fountain code is unfixed. This property is perfect suitable for the satellite channel. The satellite channel will

change rapidly with the time varying, so the traditional fixed code rate will either bring unnecessary overhead when the channel condition is good or suffer incorrect transmitting when the channel condition is bad. These two problems will be solved by the fountain code.

Another property belonging to fountain code is message recover inevitability. This property comes from that the transmitter can unstoppable encode until the receiver correctly recover the message. With this property, the navigation system will have no anxiety for the navigation signal missing problem.

2.2 LT Code

Following the concept of the rateless, Luby propose the first rateless code, namely Luby transform (LT) code. The encoding of LT code contains four steps as following:

- Step 1: The transmitter divide the original message into k packets with equal length: l bits each packet. Padding 0 if the last packet is not long enough.
- Step 2: The transmitter randomly picks degree d according to the degree distribution $\rho = (\rho_1, \rho_2, \ldots, \rho_k)$, which $p(d = i) = \rho_i$.
- Step 3: Random picking d packets from the divided k pickets.
- Step 4: Output a transmitting packet by doing XOr operation for the d picked packets.

The transmitter will continually generate encoded packets until all the transmitting packages are recovered. In theoretical, the transmitter can generate infinity encoding packets. However, the generated packets number is a little larger than k in practical, but this number is uncertain. Thus, the rate of the code is also an uncertain number, namely rateless.

Then we move on to introduce the decoding part of LT code. Belief propagation (BP) algorithm has been shown as an accepted efficient method to decode LT. The BP algorithm is based on the tanner graph of LT code, and we have given a sample example in Fig. 1. Recall the Step 4 in encoding algorithm, the tanner graph is defined by connecting the encoded packets with its constituted source packets.

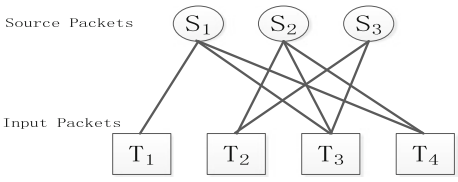

Fig. 1 Tanner graph for LT code

After transmission, the encoded packets will become the input packets of the decoder, so we rename such packets as input packets in the following discussion.

Based on this graph, we introduce the decoding algorithm as following steps:

- Step 1: Find the input packet with one-connected source packet. If there is no one-connected input packets, the decoder will wait for more input packets.
- Step 2: If one-connected packet exists, recovering the source packet as the input packet. In the previous example, T_1 is the one-connected input packet connecting to S_1, so the source packet S_1 will be decoded as T_1.
- Step 3: Delete the recovered source packet and reset the input packets by X or operation which connected to it.
- Step 4: Update the tanner graph.
- Step 5: Repeat Step 1 to Step 4 until all the source packets are recovered.

The one-connected input packet is come from the degree-one packet in encoding process. Consequently, the degree distribution will directly influence the tanner graph. That means the optimization of the degree distribution design will increase the decoding successful probability. For this reason, a lot of works have focused on to propose novel optimized degree distribution just as former mentioned. However, the research on degree distribution has met the bottleneck, in this paper we will give an optimal encoding algorithm rather than the degree distribution. We will leave the optimization of the degree distribution for satellite communication as the future work of this paper.

3 Modification for the LT Code Encoding Algorithm

We have briefly introduced the encoding and decoding algorithm of LT code in the previous section. With former discussion of the LT code, we can see that the transmission efficiency is mainly depended on the design of the degree distribution. However, the research on degree distribution has suffered bottleneck in the last few years. The new designed degree distribution cannot marginally increase the encoding efficiency. Consequently, other approaches must be raised to improve the LT code. Under such motivation, we first analyze the LT encoding algorithm in detail, and then propose a new algorithm to achieve better performance. Here we have a note that the encoding algorithm of the Raptor code is mainly based on LT encoding, hence the improvement of LT Encoding algorithm will undoubtedly increase the transmission efficiency.

3.1 Analysis for the LT Encoding Algorithm

In the previous section, we have introduced the encoding algorithm for LT code. From the discussion, we clearly see that different degree distribution function leads

to different performance. Focusing on Robust Soliton distribution, we first analyze the encoding and decoding performance.

The Robust Soliton distribution is shown as follows:

$$\mu(d) = \frac{\rho(d) + \tau(d)}{\sum_d (\rho(d) + \tau(d))}, \tag{1}$$

where $\rho(d)$ is the Ideal Soliton distribution as

$$\rho(d) = \begin{cases} 1/K & d = 1 \\ \frac{1}{d(d-1)} & d = 2, 3, \ldots, K \end{cases}, \tag{2}$$

and $\tau(d)$ is:

$$\tau(d) = \begin{cases} \frac{S}{K}\frac{1}{d}, & d = 1, 2, \cdots, \frac{K}{S} - 1 \\ \frac{S}{K}\log\left(\frac{S}{\delta}\right), & d = \frac{K}{S} \\ 0, & d > \frac{K}{S} \end{cases}. \tag{3}$$

In Eq. (3), δ is the allowed decoding failure possibility, which is a forecasting number. Usually, δ is a very small number for satellite communication, like $\delta = 0.01$. S is defined as: $S \triangleq c\sqrt{K}\ln(K/\delta)$, where c is a constant. In theoretical, c can be chosen as any real number, but we usually choose $c < 1$ in practical. Actually, choosing of c determines the performance of LT code crucially. However, theoretical analysis of determining c is still a hard problem, therefore we demonstrate the choosing of factor c with fixed δ by following simulation result in Fig. 2.

We simulate the decoding successful probability with receive packets under different c. The original packet is set as 1000. With the simulation results as shown

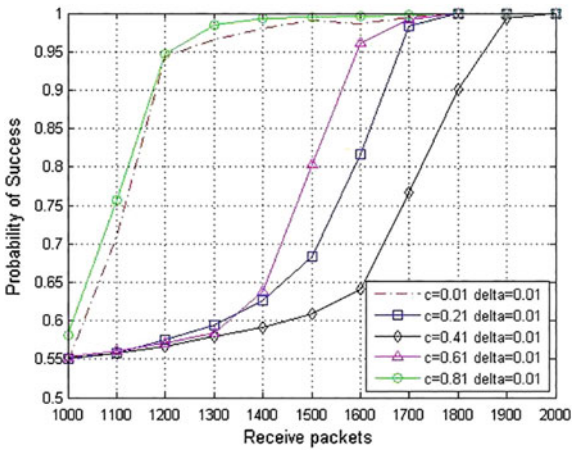

Fig. 2 Successful probability comparison with different c

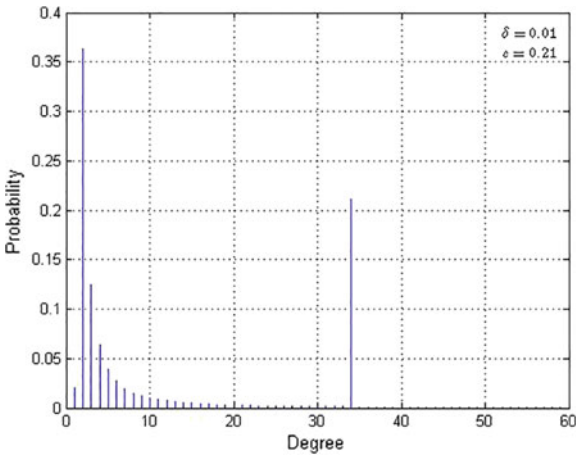

Fig. 3 Robust soliton distribution with $\delta = 0.01$ and $c = 0.21$

in Fig. 2, we can see that for Robust Soliton distribution, an optimal performance can be achieved as c = 0.81. Although this result cannot be proved by theoretical analysis yet, this simulation is be of great value as a guide to implementation.

Following the simulation instruction, we draw the Robust Soliton distribution with $\delta = 0.01$ and c = 0.81 in Fig. 3. With that we can clearly see that degree = 2 is the most frequently chosen degree; therefore, the modification of the encoding algorithm under degree 2 case will be of great value. Then we move on to propose a novel algorithm aiming at improving LT encoding performance under degree 2 case.

3.2 Modified Algorithm for LT Code Encoding

With the analysis in the last subsection, we show that the degree 2 situation case contains over quarters of the encoded packets for robust degree distribution. If we could promote the encoding efficiency for degree 2 situation, the LT encoding algorithm will be undoubtedly improved.

Fixing the degree distribution, another factor also plays an essential role to enhance LT performance, i.e., packets covering ratio. This ratio means how quickly the encoded packets will cover all the original packets. This factor is significant with the reason that all original packets must be covered, otherwise the receiver cannot recover all original packets. Consider the situation that the well-designed degree distribution has provided enough available decoding packets in each round; however, one of the original packets has never been chosen to be transmitted. Under such situation, the decoding is still a failure. Accordingly, covering the whole original packets as soon as possible will be effective to reduce the transmitting packets cost.

Recalling the degree 2 situation, we have shown that this situation occupies over quarters of whole transmitting packets. Thus, improving the packets covering ratio under degree 2 will be of great value. Assuming K packets are transmitted, so primary encoding algorithm costs $\binom{K}{2}$ solutions to pick 2 packets from the K packets. To reduce such cost, we predivide the K packets into two groups and picking one from each. For this proposal, only $\binom{K}{1} * \binom{K}{1}$ are cost. Taking $K = 10,000$ as an example, primary encoding algorithm has 49,995,000 solutions, however, the improved algorithm only cost 25,000,000 which is less than the half of the primary algorithm.

The modified encoding algorithm has been shown as follows:

Algorithm: ***Modified Algorithm for LT Code Encoding***

Input: Original Data S, Degree Distribution ρ, Data Packets Number K
Output: Encoded Packets T

procedure ENCODING(S, ρ, K)
  Divide Original Data S into K Packets $\{S_1, S_2, \cdots, S_K\}$, padding 0 if bits lack.
  Divide Packets $\{S_1, S_2, \cdots, S_K\}$ into two gourps S_A, S_B
  $i \leftarrow 1$
  repeat
    Picking Degree d based on Degree Distribution ρ
    if $d = 2$ **then**
      Seperately choosing u_1 from S_A and u_2 from S_B
    else
      Rondomly nonrepeated chooing $u_1, u_2, \cdots, u_d$ from packages.
    end if
    $T_i \leftarrow u_1 \oplus u_2 \oplus \cdots \oplus u_d$
    $i \leftarrow i + 1$
  until Recieving Correct Decoding ACK
end procedure

4 The Application of Fountain Code in Satellite Navigation System

The fountain code was first analyzed in the erasure channel with an impressive performance. Further, some researchers extend its application into other channel models as former mentioned. Meanwhile, some features belonging to fountain code,

like rateless, message recover inevitability are exactly fit the satellite channel model. Then it is a natural thought that applying the fountain code into satellite navigation system.

4.1 The Advantage Analysis of Applying Fountain Code into Satellite Navigation System

Before we analyze the advantage, we first discuss about the channel properties of the satellite navigation signal.

Two main problems are needed to be deal with the navigation signals. The first problem is the signal distortion caused by the interference from ionosphere, troposphere, and local surface. The second problem is the frequent consecutive burst errors, such errors often request large number of redundancies to preventing transmission failure.

To deal with such problems, the fountain code is an optimal candidate comparing with current applying channel code like LDPC in GPS L1C. The reasons are as follows. First, the message recovers inevitability of fountain code can guarantee the transmission success. Causer transmitter will unstop to generate transmitting packets until all the packets are recovered. Second, the rateless feature can reduce the former mentioned redundancy. Facing the situation that frequent burst errors often happen, the fixed rate must reserve enough redundancies. However, such redundancies will be unnecessary when the channel condition is good. Thus, the rateless code, i.e., fountain code, will improve such waste.

4.2 Preliminaries for Low-Earth Orbit Satellite

With former analysis, we can directly see that fountain code is perfectly suitable for satellite navigation system. Besides naive transplanting, a recently conducted experiment in November by NASA provides a brand-new prospect. In that experiment, LEo satellite is utilized to assistant GPS signal transmitting. This experiment also forecast that using LEo satellite could be an effective approach to improve the quality of navigation signals.

The Low-Earth orbit satellite is the satellite that occupies the orbit around earth with the altitude between 180 and 1240 km. With a closer distance from the Earth's surface, the LEo satellite enjoys a better communication than the Medium-Earth orbit satellite where almost all navigation satellites are belonging to GPS, Galileo, and Beidou.

4.3 The Application of Fountain Code in Satellite Navigation System

We combine two key techniques to realize an equivalent ensure channel, namely concatenated code and LEo satellites which has been introduced in last subsection. Further, such equivalent ensures channel that will be perfect for the application of fountain code in satellite navigation system.

The concatenated code was first presented by Forney in 1966 by naive concatenating block code and cyclic code. Forney also prove that the performance improvement would only be with polynomial-time decoding complexity that is increasing. Following this idea, we concatenate the fountain code with error-correcting code. Rather than directly concatenating, we separate the two encoders in different satellite to form an equivalent ensure channel.

In the transmitter, i.e., the navigation satellite, the original message will be first divided into packets. Then the transmitter encodes these packets with fountain code encoding. The navigation satellite will transmit these coded packets to the LEo satellite. The LEo satellite will not decode these packets, instead it will do the second-time encoding. LDPC or turbo code is suggested. After the inner encoding, LEo will forward the packets to the receiver. Here is a note that interleaving is needed for LDPC against the emerging of burst errors.

The decoders, both the inner and outer, are lying at the receiver. Rather than the routine sequential decoding, we have different designs. The decoder will first detect the error for the inner code, and make a judgment. If these errors are in the threshold, the inner decoder will correct them. Otherwise, this packet will be ensured. Thus, an equivalent ensures that the channel is generated for the outer code, which will be fountain code in our scheme. The inner decoder will send the corrected packets into the outer decoder to accomplish the fountain code decoding. Waiting for the all original packets recovered, the receiver will send a ACK to the transmitter to finish this round of message transmitting.

The transmission diagram is shown in Fig. 4.

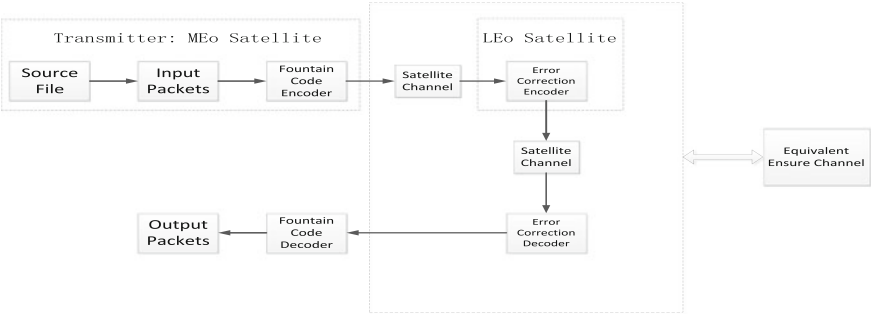

Fig. 4 Transmission diagram of proposed concatenated code

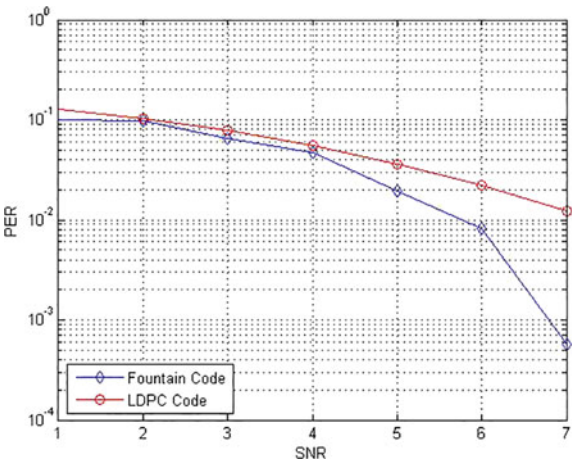

Fig. 5 Packets error ratio comparison for fountain code with LDPC code

4.4 Simulation Result of LT-LDPC Concatenated Code

To perform the proposed concatenated fountain code scheme, we simulate the situation by comparing the packet error ratio (PER) between the proposed code with LDPC which is used in GPS L1C. We choose LT code as the outer code and LDPC code as the inner code. We consider that 1000 packets has been transmitted, and set the rate of LDPC code as 0.5. Correspondingly, we assume 2000 packets have been received.

The simulation result is shown in Fig. 5. With the result we can see that with fixed SNR, the proposed code can correct more errors than LDPC code especially in high SNR region. Further, the ratelss and message recover inevitability feature belonging to fountain code makes it perfect suitable for the satellite navigation system.

5 Conclusions

The navigation signal is a significant factor to influence the quality of navigation service. However, the signal will suffer a bad distortion due to the satellite communication features. To deal with this problem, we apply the fountain code into navigation system. First, we briefly overview the fountain code with two practical scheme, namely LT code and Raptor code. Second, we modified the encoding algorithm of LT code to reduce the transmitting packets cost. At last, we apply the fountain code into navigation system with the help of LEo.

Some future work can be considered as follows. First, a novel degree distribution is desired for the particular satellite communication. Second, determining the factor c with theoretical analysis in Robust Soliton distribution is also a promising

way to improve the fountain code. And last, to improve the application in navigation system, different concatenated code approaches should be analyzed to seek out the optimal one.

Acknowledgments This work is supported by National Natural Science Foundation of China (No. 61101147), The National Basic Research Program of China (973 Program, No. 2012CB316100), Specialized Research Fund for Doctoral Program of Higher Education (No. 20110203120004), Natural Science Basic Research Plan in Shaanxi Province of China (Program No.2014JZ018), Science Research Plan in Shaanxi Province of China (No. 2013K06-15), The Fundamental of Research Funds for the Central Universities (No. K5051301006), The 111 Project (No. B08038), National Natural Science Foundation (No. 61472308)

References

1. Cassuto Y, Shokrollahi A (2015) Online fountain codes with low overhead. IEEE Trans Inf Theory 61(6):3137–3149
2. Hanzo L, Maunder RG, Chen H, Tafazolli R, Ma Y (2015) Hybrid-ARQ-aided short fountain codes designed for block-fading channels. IEEE Trans Veh Technol 99:1–12
3. Hussain I, Land I, Chan TH, Xiao M, Rasmussen LK (2014) A new design framework for LT codes over noisy channels. In: 2014 IEEE international symposium on information theory (ISIT). IEEE, pp 2162–2166
4. Luby M (2002) LT codes. In: Proceedings of the 43rd symposium on foundations of computer science. IEEE Computer Society
5. Shokrollahi A (2006) Raptor codes. IEEE Trans Inf Theory 52(6):2551–2567
6. Yen KK, Liao YC, Chen CL, Chang HC (2013) Modified robust soliton distribution (MRSD) with improved ripple size for LT codes. IEEE Commun Lett 17(5):976–979
7. Yue J, Lin Z, Vucetic B (2014) Distributed fountain codes with adaptive unequal error protection in wireless relay networks. IEEE Trans Wireless Commun 13(8):4220–4231
8. Zhang Q, Zhang S, Zhou W (2014) Enhanced LT decoding scheme in satellite communication. In: 2014 sixth international conference on wireless communications and signal processing (WCSP). IEEE, pp 1–6

A Comprehensive Evaluation Approach of Navigation Signal Performance Based on Multi-attribute Group Decision Making

Qing Liu, Yanhong Kou and Zhigang Huang

Abstract In the process of comprehensive performance evaluation of new-structure satellite navigation signals, some problems may be encountered including the wide varieties of performance indicators/attributes, the lack of a clear attribute system, the complex relationships and strong correlations among different attributes, the differences in user preferences of the significances of various attributes, and so on. Based on the comparative analysis of different models and methods for the fuzzy multi-criteria Group Decision Making (GDM) problems, this paper proposes a comprehensive signal performance evaluation approach that integrates multiple methods seamlessly. Firstly, a three-level signal attribute system is established based on Analytic Hierarchy Process (AHP). Next, the attributes at the bottom level are decorrelated and reconstructed by Fuzzy Clustering and Principal Component Analysis (PCA). Then the Technique for Order Preference by Similarity to Ideal Solution (TOPSIS) is employed to obtain the Relative Membership Degree (RMD) of each alternative signal option to each attribute unit. Finally, the overall performance of each alternative is calculated using the multi-attribute GDM model. The evaluation of six alternative modulations for GPS L1C signals based on theoretical analysis demonstrates the feasibility and effectiveness of the proposed approach. The approach provides an efficient means for the comprehensive performance evaluation of satellite navigation signals.

Keywords Satellite navigation signal · Multi-attribute group decision making · AHP · PCA · TOPSIS · Fuzzy clustering

Q. Liu · Y. Kou (✉) · Z. Huang
School of Electronic and Information Engineering, Beihang University, Beijing 100191, China
e-mail: kouy@buaa.edu.cn; xc1989love@buaa.edu.cn

J. Sun et al. (eds.), *China Satellite Navigation Conference (CSNC) 2016 Proceedings: Volume II*, Lecture Notes in Electrical Engineering 389,
DOI 10.1007/978-981-10-0937-2_2

1 Introduction

With the development of Global Navigation Satellite System (GNSS), various novel navigation signal structures have been proposed. Signal structure design is one of key tasks of GNSS design, and the scientific and comprehensive performance evaluation of different signal structures becomes of great importance for the achievement of function and performance goals of GNSS services.

Multi-criteria/multi-attribute decision making (MCDM/MADM) approaches have been widely applied in the fields of military affairs, transportation, healthcare, mining, hydraulic engineering, and so forth [1–7]. Nevertheless, few literatures can be found about applying these approaches in the evaluation of GNSS signal performances. Several related methods for GNSS signal performance evaluation have been mentioned/studied in [8], including the radar chart method, the expert scoring method, the linear weighting method, and the weighted Technique for Order Preference by Similarity to Ideal Solution (TOPSIS). These methods, however, need to be improved due to their inefficiency of dealing with subjectivity, lack of consideration of correlations among the attributes, or lack of quantitative analysis.

In order to solve these problems, this paper first establishes a hierarchical attribute system for satellite navigation signals. The signal attribute system can be divided into the following three levels: (1) The bottom level is composed of all the computable/measurable performance indicators, i.e., the attributes; (2) The middle level classifies these attributes into several groups, with one group named as an Attribute Unit (AU); (3) The top level forms the Group Decision Making (GDM) target and represents the overall performance of the signal. Then a fuzzy comprehensive evaluation approach is explored to act as the technical means for the optimal selection of signal alternatives, which takes advantage of Analytic Hierarchy Process (AHP), Principal Component Analysis (PCA), Fuzzy Clustering and weighted TOPSIS appropriately. Finally, taking six GPS L1C signal modulation alternatives as a case study [9], the evaluation results select the TMBOC (6,1,4/33) modulation meeting with the interface specification document IS-GPS-800.

2 Methodology

The proposed evaluation approach includes the following three steps: (1) to establish the three-level architecture of the signal attribute system for AHP; (2) to calculate the Relative Membership Degree (RMD) of each alternative signal option with respect to each AU; (3) to calculate the overall RMD of each alternative signal option.

2.1 Signal Attribute System

There is a wide range of attributes indicating different performances of satellite navigation signals. On the other hand, the relative importance of these attributes can vary significantly for different users and applications. As one of the most popular analytical techniques for complex decision making problems, AHP is firstly considered in our methodology to well characterize the signal option decision situation and efficiently incorporate objective as well as subjective attributes into the decision. Taking account of the definition, application requirements, and relevance of these attributes, as well as the summary of available theoretical data and test data for different signal options, a three-level signal attribute system is established for the decision making among different signal alternatives, as shown in Fig. 1. The specific attributes corresponding to the raw measurement/analysis data fall into the bottom level. The second level attributes can be obtained by classifying the first-level attributes with similar characteristics into an AU, such as the anti-interference capability, the measurement accuracy, the receiving threshold, and so forth. The third (top) level is the overall performance indicator corresponding to the evaluation result. This hierarchical architecture helps to reduce the workload, difficulty, subjectivity, and arbitrariness for the Experts, User representatives, and Decision makers (EUD) to assign weights to different attributes because only a few second-level attributes need to be weighted or, more simply, pairwisely compared according to the application preferences.

2.2 Fuzzy Optimization Model of One AU

The fuzzy optimization model of one AU includes the following two steps: decorrelation of the attributes and calculation of the RMD of each alternative to each AU.

2.2.1 Decorrelation of Attributes

Correlations among the attributes can be captured and reduced by employing fuzzy clustering and PCA.

AU Fuzzy Clustering

The attribute value (measured/calculated/estimated data) matrix for the decision problem with m attributes of the kth AU and n alternatives can be expressed as Eq. (1):

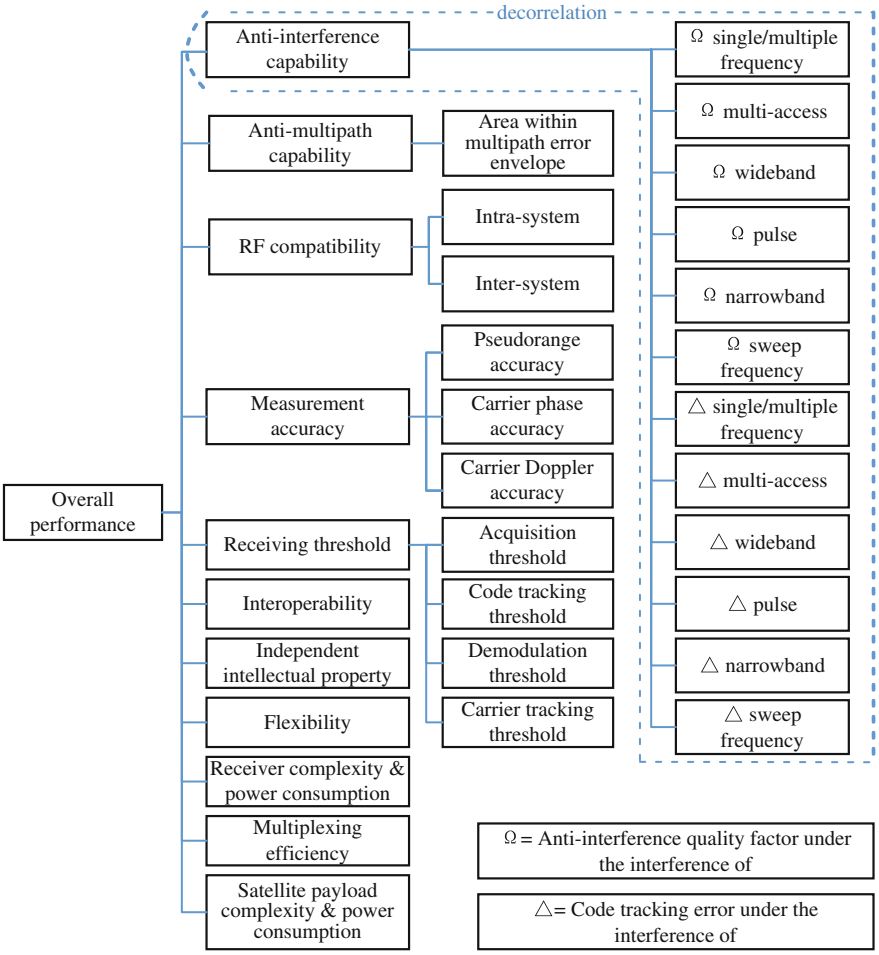

Fig. 1 Attribute system of satellite navigation signal

$$ {}_{1k}X = \begin{bmatrix} {}_{1k}x_{11} & {}_{1k}x_{12} & \cdots & {}_{1k}x_{1m} \\ {}_{1k}x_{21} & {}_{1k}x_{22} & \cdots & {}_{1k}x_{2m} \\ \vdots & \vdots & \vdots & \vdots \\ {}_{1k}x_{n1} & {}_{1k}x_{n2} & \cdots & {}_{1k}x_{nm} \end{bmatrix} = \left({}_{1k}x_{ij}\right)_{n\times m} \tag{1} $$

where $i = 1, 2, \ldots, n$; $k = 1, 2, \ldots, t$; $j = 1, 2, \ldots, m$; ${}_{1k}x_{ij}$ denotes the attribute value at the first level.

To make the attributes dimensionless and larger-the-better, the raw attribute value matrix can be normalized as follows:

$$ {}_{1k}X' = \begin{bmatrix} {}_{1k}x'_{11} & {}_{1k}x'_{12} & \cdots & {}_{1k}x'_{1m} \\ {}_{1k}x'_{21} & {}_{1k}x'_{21} & \cdots & {}_{1k}x'_{2m} \\ \vdots & \vdots & \vdots & \vdots \\ {}_{1k}x'_{n1} & {}_{1k}x'_{n1} & \cdots & {}_{1k}x'_{nm} \end{bmatrix} = \left({}_{1k}x'_{ij} \right)_{n\times m} \tag{2} $$

where

$$ {}_{1k}x'_{ij} = \frac{{}_{1k}x_{ij} - \overline{{}_{1k}x_j}}{{}_{1k}S_j} \quad \text{if attribute } j \text{ is a utility-type attribute} \tag{3} $$

$$ {}_{1k}x'_{ij} = 1 - \frac{{}_{1k}x_{ij} - \overline{{}_{1k}x_j}}{{}_{1k}S_j} \quad \text{if attribute } j \text{ is a cost-type attribute} \tag{4} $$

$$ \begin{aligned} \overline{{}_{1k}x_j} &= \frac{1}{n}\sum\nolimits_{i=1}^{n} {}_{1k}x_{ij} \\ {}_{1k}S_j &= \sqrt{\frac{1}{n}\sum\nolimits_{i=1}^{n} \left({}_{1k}x_{ij} - \overline{{}_{1k}x_j} \right)^2} \end{aligned} \tag{5} $$

The correlation matrix of Eq. (2) is calculated as

$$ {}_{1k}R = \left({}_{1k}r_{ij} \right)_{m\times m},\ {}_{1k}r_{ij} = \frac{\mathrm{cov}\left({}_{1k}x_i, {}_{1k}x_j \right)}{\sqrt{D\left({}_{1k}x_i \right) D\left({}_{1k}x_j \right)}} \tag{6} $$

Generally, since ${}_{1k}R$ is not a fuzzy equivalent matrix, its transitive closure ${}_{1k}R'$ should be further computed. By comparing the elements of ${}_{1k}R'$ with a threshold ${}_{1k}\lambda$, a matrix ${}_{1k}R'_{\lambda}$ with binary elements (0 or 1) is obtained. The attributes with value of 1 in one row/column can be classified into the same cluster.

The clustering results depend on the value of ${}_{1k}\lambda$. Assuming that ${}_{1k}R'_{\lambda}$ divides one AU into m_k clusters, $c_1, \ldots, c_l, \ldots, c_{m_k}$, where c_l $(l = 1, \ldots, m_k)$ represents the lth cluster, the evaluation objective function of ${}_{1k}\lambda$ can be estimated by Wang et al. [6]:

$$ {}_{1k}S = {}_{1k}\delta / {}_{1k}L \tag{7} $$

where ${}_{1k}\delta$ is the average Hamming distances [10] between the cluster centers and all the sample attributes, ${}_{1k}L$ is the minimum distance between different cluster centers. By choosing the best ${}_{1k}\lambda$ corresponding to the smallest ${}_{1k}S$, efficient and reasonable clustering can be achieved.

Construction of Composite Attribute of Each Cluster based on PCA

After the process of fuzzy clustering, it is essential to construct a new attribute for each cluster, which represents the composite performance of all the attributes in the cluster. The attribute values of the lth cluster of the kth AU are regrouped as

$$ {}_{1k}X'' = \begin{Bmatrix} {}_{1k}x''_{11} & \cdots & {}_{1k}x''_{1m_c} \\ \vdots & \ddots & \vdots \\ {}_{1k}x''_{n1} & \cdots & {}_{1k}x''_{nm_c} \end{Bmatrix} \tag{8} $$

where n is the number of the alternatives, m_c is the number of the attributes in this cluster, ${}_{1k}x''_{ij}$ keeps the attribute value of ${}_{1k}x'_{ij}$ in Eq. (2) and is reordered in the cluster. Normalizing Eq. (8) leads to ${}_{1k}Z = ({}_{1k}z_{ij})_{n\times m_c}$, where

$$ {}_{1k}z_{ij} = \frac{{}_{1k}x''_{ij} - \overline{{}_{1k}x''_j}}{{}_{1k}S''_j} \tag{9} $$

And

$$ \overline{{}_{1k}x''_j} = \frac{1}{n}\sum\nolimits_{i=1}^{n} {}_{1k}x''_{ij} $$

$$ {}_{1k}S''_j = \sqrt{\frac{1}{n}\sum\nolimits_{i=1}^{n}\left({}_{1k}x''_{ij} - \overline{{}_{1k}x''_j}\right)^2} $$

Thus the jth column vector of the normalized matrix has a zero mean and a unit variance $E({}_{1k}Z_j) = 0,\ D({}_{1k}Z_j) = 1$.

The correlation matrix of ${}_{1k}Z$ is

$$ {}_{1k}R_z = ({}_{1k}r_{ij})_{m_c\times m_c} = \frac{1}{n-1}\,{}_{1k}Z^T\,{}_{1k}Z \tag{10} $$

$$ {}_{1k}r_{ij} = \mathrm{cov}({}_{1k}Z_i, {}_{1k}Z_j) \tag{11} $$

Assuming that ${}_{1k}R_z$ has q eigenvalues greater than zero $(\lambda_1, \lambda_2, \cdots, \lambda_q)$, $\lambda_i > 0$, and the corresponding orthonormal eigenvectors are $A = (a_1, a_2, \cdots, a_q)$, q principal components can be computed by

$$ Y_{n\times q} = (y_1, y_2, \ldots, y_q) = {}_{1k}Z_{n\times m_c}A_{m_c\times q} $$

$$ \begin{bmatrix} y_{11} & \cdots & y_{1q} \\ \vdots & \ddots & \vdots \\ y_{n1} & \cdots & y_{nq} \end{bmatrix} = \begin{bmatrix} {}_{1k}z_{11} & \cdots & {}_{1k}z_{1m_c} \\ \vdots & \ddots & \vdots \\ {}_{1k}z_{n1} & \cdots & {}_{1k}z_{nm_c} \end{bmatrix} \begin{bmatrix} a_{11} & \cdots & a_{1q} \\ \vdots & \ddots & \vdots \\ a_{m_c1} & \cdots & a_{m_cq} \end{bmatrix} \tag{12} $$

As indicated by Yu [11], the principal components in Eq. (9) are independent

$$ \mathrm{cov}(y_i, y_j) = \begin{cases} 0 & i \neq j \\ \lambda_i & i = j \end{cases} \tag{13} $$

The contribution of the principal component y_i to the total variance is estimated as

$$\omega_i = \lambda_i \Big/ \sum_{j=1}^{q} \lambda_j \tag{14}$$

Ranking $y_1, y_2, \ldots, y_q$ in the descending order of $\omega_1 > \omega_2 > \cdots \omega_q$, the cumulative variance contribution of the first m_ρ principal components is:

$$\rho = \sum_{i=1}^{m_\rho} \lambda_i \Big/ \sum_{j=1}^{m_c} \lambda_j \tag{15}$$

Different value of ρ yield different reconstructed attribute $x_l^{new} = \sum_{i=1}^{m_\rho} \omega_i y_i$ as the composite performance evaluation of the lth cluster. In addition, large ρ allows more information kept in the newly constructed attribute.

If several clusters have been generated in the fuzzy clustering process for an AU, the above process should be repeated to reconstruct a separate attribute for each cluster.

2.2.2 Calculation of RMD to Each AU Based on Weighted TOPSIS

After the decorrelation of the attributes, a new attribute value matrix $\left({}_{1k}x^{\text{new}}\right)_{n\times m_k}$ for the kth AU is obtained. The weights of these reconstructed attributes can be determined by Wang [2]

$${}_{1k}\omega_j = \sum_{i=1}^{n} {}_{1k}rr_{ij}^{\text{new}} \Big/ \sum_{i=1}^{n}\sum_{j=1}^{m_k} {}_{1k}rr_{ij}^{\text{new}} \tag{16}$$

where ${}_{1k}\omega_j$ denotes the weight of the jth attribute of the kth AU, and ${}_{1k}rr_{ij}^{\text{new}} = \frac{{}_{1k}x_{ij}^{\text{new}} - \min_i\left\{{}_{1k}x_{ij}^{\text{new}}\right\}}{\max_i\left\{{}_{1k}x_{ij}^{\text{new}}\right\} - \min_i\left\{{}_{1k}x_{ij}^{\text{new}}\right\}}$ is the RMD of ${}_{1k}x_{ij}^{\text{new}}$.Using this objective weighting method, the trouble and arbitrariness of subjective weighting of a large number of attributes can be avoided.

According to the optimization rule of minimizing the sum of squares of the weighted distances to both the ideal and negative ideal solutions, the RMD of the ith alternative to the kth AU can be calculated by Wang [12]

$$u_{ik} = 1 \Big/ \left(1 + \left\{\sum_{j=1}^{m_k}\left[\omega_j\left(1 - {}_{1k}rr_{ij}^{\text{new}}\right)\right] \Big/ \sum_{j=1}^{m_k}\left[\omega_j \cdot {}_{1k}rr_{ij}^{\text{new}}\right]\right\}^2\right) \tag{17}$$

Equation (17) is the fuzzy optimization result representing the composite performance of each alternative to one AU. For an AU without decorrelation process, the same process of weighting and calculation of the RMD as shown Eqs. (16)–(17) can be conducted.

2.3 Multi-level Multi-attribute GDM Model

This model will output the final evaluation results by performing the following two steps: (1) assembly of the weights of attributes at the second level of AHP according to the judgements of all the EUDs; (2) calculation of the overall performance RMD of each alternative signal option.

2.3.1 Group Decision of Weights of AUs

In the previous section, one attribute for one AU has been obtained. The t attributes at the second level of signal attribute system are denoted as $O = \{o_1, o_2, \ldots, o_t\}$. Scaling the relative importance of the attributes using the Fuzzy degree value defined in Table 1, the Pairwise Comparison Matrix (PCM) [13] can be obtained

$$\beta = \begin{bmatrix} \beta_{11} & \beta_{12} & \cdots & \beta_{1t} \\ \beta_{21} & \beta_{22} & \cdots & \beta_{2t} \\ \vdots & \vdots & \vdots & \vdots \\ \beta_{t1} & \beta_{t2} & \cdots & \beta_{tt} \end{bmatrix} \tag{18}$$

where $\beta_{kl} = 1 - \beta_{lk}$ denotes the importance fuzzy degree of o_k relative to o_l. When o_k is more important than o_l, $0.5 < \beta_{kl} < 1$; when o_k and o_l are of the same importance, $\beta_{kl} = 0.5$; Otherwise $0 < \beta_{kl} < 0.5$.

The mood operators in Table 1 comes from the judgments of the EUDs. Since the navigation signals of different frequencies lay particular stress on different applications, different EUDs may be endowed with different weights for a specified signal. Assuming that α_k $(k = 1, \ldots, p)$ is the weight of the kth EUD and β_k represents the PCM given by the kth EUD, the p PCMs can be assembled by linear weighting

$$\bar{\beta} = \sum_{k=1}^{p} \alpha_k \beta_k \tag{19}$$

Table 1 Pairwise comparison scale of attributes according to mood operator

MO of the relative importance	Equally	Slightly more	Moderately more	Strongly more	Extremely more	Absolutely
FD	0.50	0.60	0.70	0.80	0.90	0.10

Annotation "MO" represents "mood operator", "FD" represents "fuzzy degree"

The normalized sum of a row in the matrix $\bar{\beta}$ represents the relative importance of the corresponding attribute

$$W_i' = \sum_{j=1}^{t} \bar{\beta}_{ij}, \quad i = 1, 2, \ldots t;\ i \neq j \tag{20}$$

$$W_i = W_i' \Big/ \sum\nolimits_{i=1}^{t} W_i' \tag{21}$$

Thus the weight vector of the t AUs is $W = (W_1, W_2, \cdots, W_t)^T$.

2.3.2 Calculation of Overall Performance RMD

Now that the RMD of each alternative corresponding to each AU has been given by Eq. (17) and the weight of each attribute given by Eq. (23), the final decision making vector can be obtained by simple linear weighting

$$U_{n\times 1} = \begin{bmatrix} U_1 \\ U_2 \\ \vdots \\ U_n \end{bmatrix} = \begin{bmatrix} u_{11} & u_{12} & \cdots & u_{1t} \\ u_{21} & u_{22} & \cdots & u_{2t} \\ \vdots & \vdots & \vdots & \vdots \\ u_{n1} & \cdots & \cdots & u_{nt} \end{bmatrix} \begin{bmatrix} W_1 \\ W_2 \\ \vdots \\ W_t \end{bmatrix} \tag{22}$$

where u_{ij} is the RMD of the ith alternative corresponding to the jth AU; U_i is the overall performance RMD of the ith alternative. So, the alternative with the maximum value of U_i represents the optimal signal option with the best overall performance.

3 Case Study

Taking the selection of GPS L1C signal modulation scheme as a case study, this section shows the evaluation process of the following six signal modulation options: BPSK(1), BPSK(2), BOC(1,1), TMBOC(4,1,4/33), TMBOC(5,1,4/33), and TMBOC(6,1,4/33). The raw value of each attribute is only based on theoretical calculation, with the preconditions and the attribute values shown in Tables 2 and 3 respectively. Note that only parts of the attributes in Fig. 1 have been taken into account. As shown in the first column of Table 3, the attributes have been grouped into six AUs. Additionally, the interoperability performance is calculated using the method proposed by Liu [14], and other attribute values are obtained according to the methods introduced in [15].

Table 2 Preconditions of theoretical calculation of signal performance

Parameter	Considerations	Value
Front-end bandwidth	Main lobe bandwidth of the signal	Main lobe bandwidth
Correlator spacing	$d < v/(2u)$	0.08 chip
DLL bandwidth	Typical receiver design	1 Hz
PLL bandwidth	Typical receiver design	15 Hz
Integration time	One code period	10 ms
Carrier to noise ratio (C/N0)	Nominal signal power level and thermal noise background	44 dB-Hz
Multipath to direct path ratio (MDR)	Typical value for test and analysis	−6 dB
L1 C/A signal power	Typical value for test and analysis of intra-system RF compatibility	−128.5 dBm
Interference to signal power ratio (C_I/C_s)	Typical value for test and analysis	40 dB
Interference	Typical parameters for test and analysis	Wideband: bandwidth covering signal main lobe
		Narrowband: 5 % of the main lobe bandwidth
		Pulse: 2 ms period, 200 us duration
		Single frequency: center frequency of the signal
		Sweep frequency: 1 kHz step, 1 ms period

Annotation "v" and "u" are originated from $BOC(u, v)$ signal parameters

The PCMs given by four user representatives has been assembled into

$$\beta = \begin{pmatrix} 0.5 & 0.45 & 0.6 & 0.25 & 0.35 & 0.65 \\ 0.55 & 0.5 & 0.65 & 0.3 & 0.4 & 0.7 \\ 0.4 & 0.35 & 0.5 & 0.15 & 0.25 & 0.55 \\ 0.75 & 0.7 & 0.85 & 0.5 & 0.6 & 0.9 \\ 0.65 & 0.6 & 0.75 & 0.4 & 0.5 & 0.8 \\ 0.35 & 0.3 & 0.45 & 0.1 & 0.2 & 0.5 \end{pmatrix} \tag{23}$$

Thus the weight vector of the 6 AUs is:

$$\omega = (\,0.1556 \quad 0.1722 \quad 0.1222 \quad 0.2389 \quad 0.2056 \quad 0.1056\,) \tag{24}$$

The 12 anti-interference attributes of the first AUs in Table 3 need to be decorrelated and reconstructed. According to Eqs. (2)–(6), the correlation matrix of the 12 raw attributes is

Table 3 Theoretical value of each attribute

Modulation / Attribute	BPSK (1)	BPSK (2)	BOC (1,1)	TMBOC (4,1,4/33)	TMBOC (5,1,4/33)	TMBOC (6,1,4/33)
Δ wideband (m)	12.78	4.00	3.17	0.86	0.66	0.54
Δ narrowband (m)	0.38	0.97	0.22	0.21	0.18	0.18
Δ single frequency (m)	1.37	0.59	5.99	1.56	1.24	1.05
Δ multi-access (m)	12.78	4.008	4.22	1.16	0.96	0.78
Δ pulse (m)	1.73	0.62	0.49	0.23	0.20	0.18
Δ multi-frequency (m)	2.53	4.11	1.03	1.00	0.78	0.39
Ω wideband	1.50	1.50	4.02	6.80	7.86	8.93
Ω narrowband	10.04	10.04	24.75	11.15	9.40	8.17
Ω single frequency	1	1	2.47	2.71	2.71	2.71
Ω multi-access	1.50	1.50	3.03	3.59	3.58	4.50
Ω pulse	1	1	2.24	2.47	2.47	2.47
Ω sweep frequency	43.31	43.32	45.70	42.18	41.74	41.49
Area within multipath error envelope (chip • m)	5.72	5.72	3.66	2.38	2.39	1.82
RF compatibility (dB)	0.14	0.10	0.09	0.07	0.07	0.06
Code tracking jitter (m)	0.92	0.46	0.38	0.16	0.14	0.14
Carrier tracking jitter (°)	1.98	1.98	1.98	1.62	1.62	1.62
Code tracking threshold (dB-Hz)	31.6	31.9	25.1	19.6	19.2	19.2
Carrier tracking threshold (dB-Hz)	26.47	26.47	26.47	24.73	24.73	24.73
Interoperability	0.32	0.33	0.57	0.57	0.57	0.57

Annotation "Δ" represents "code tracking jitter under the interference of"; "Ω" represents "anti-interference quality factor under the interference of"

$$
{}_{11}R = \begin{pmatrix}
1 & 0.280 & 0.036 & 0.997 & 1.000 & 0.528 & 0.804 & -0.053 & 0.788 & 0.798 & 0.789 & -0.361 \\
0.280 & 1 & -0.347 & 0.246 & 0.280 & 0.956 & 0.796 & 0.108 & 0.802 & 0.796 & 0.802 & -0.204 \\
-0.036 & -0.347 & 1 & 0.043 & -0.054 & -0.308 & -0.214 & -0.931 & -0.342 & -0.248 & -0.335 & -0.815 \\
0.997 & 0.246 & 0.043 & 1 & 0.995 & 0.498 & 0.783 & -0.124 & 0.757 & 0.774 & 0.759 & -0.422 \\
1.000 & 0.280 & -0.054 & 0.995 & 1 & 0.530 & 0.803 & -0.038 & 0.790 & 0.799 & 0.791 & -0.344 \\
0.528 & 0.956 & -0.308 & 0.498 & 0.530 & 1 & 0.926 & 0.042 & 0.924 & 0.932 & 0.924 & -0.293 \\
0.804 & 0.796 & -0.214 & 0.783 & 0.803 & 0.926 & 1 & 0.006 & 0.991 & 0.997 & 0.992 & -0.378 \\
-0.053 & 0.108 & -0.931 & -0.124 & -0.038 & 0.042 & 0.006 & 1 & 0.143 & 0.026 & 0.136 & 0.898 \\
0.788 & 0.802 & -0.342 & 0.757 & 0.790 & 0.924 & 0.991 & 0.143 & 1 & 0.991 & 1.000 & -0.249 \\
0.798 & 0.796 & -0.248 & 0.774 & 0.799 & 0.932 & 0.997 & 0.026 & 0.991 & 1 & 0.991 & -0.346 \\
0.789 & 0.802 & -0.335 & 0.759 & 0.791 & 0.924 & 0.992 & 0.136 & 1.000 & 0.991 & 1 & -0.256 \\
-0.361 & -0.204 & -0.815 & -0.422 & -0.344 & -0.293 & -0.378 & 0.898 & -0.249 & -0.346 & -0.256 & 1
\end{pmatrix} \tag{25}
$$

It can be seen that about 50 % of the elements in Eq. (25) are larger than 0.7. In the process of fuzzy clustering the minimal ${}_{11}S = 0.178$ (with ${}_{11}\delta$=1.49 and ${}_{11}L = 8.361$) can be achieved when using ${}_{11}\lambda$=0.7. Consequently, two clusters for the anti-interference AU are generated from the raw 12 attributes. With one attribute

reconstructed for one cluster by employing PCA, the correlation matrix of the new attribute value matrix $({}_{11}x^{\text{new}})_{6\times 2}$ becomes

$$ {}_{11}R^{\text{new}} = \begin{pmatrix} 1.0 & -0.25 \\ -0.25 & 1.0 \end{pmatrix} \tag{26} $$

It can be seen that the fuzzy clustering and PCA can effectively mitigate the correlation among the attributes and reduce the number of attributes as well.

The RMDs of the six AUs are calculated using weighted TOPSIS as introduced in Sect. 2.2, and then incorporated into the multi-level multi-attribute GDM model in Sect. 3. The overall performance RMD vector of the six alternatives is

$$ U = (\,0.21 \quad 0.3094 \quad 0.3064 \quad 0.8281 \quad 0.8258 \quad 0.8521\,) \tag{27} $$

Equation (27) ranks the six signal modulation options as follows: {TMBOC (6,1,4/33), TMBOC(4,1,4/33), TMBOC(5,1,4/33), BPSK(2), BOC(1,1), BPSK(1)}. The selected TMBOC(6,1,4/33) modulation coincides with the GPS LICP signal specification in the IS-GPS-800 document.

It is important to note that the short-list of signal attributes and the values of the attributes affect the evaluation results directly. Not all the signal attributes have been considered, and only the attribute values theoretically calculated with the ideal channel assumptions are inputted to the evaluation process of the case study. In practical applications, the signal performances will be degraded by channel imperfections to different extents for different signal structures. Nevertheless, the proposed evaluation approach is still applicable to the comprehensive performance evaluation of signal structures if complete attributes and practical values of attributes are incorporated. In addition to theoretical data, the testing or measured data of signal performances can also serve as the raw attribute values.

4 Conclusion

This paper has proposed a multi-attribute GDM approach for the comprehensive evaluation of the overall performances of satellite navigation signal options. The approach is an organic combination of AHP, fuzzy clustering, PCA, weighted TOPSIS, and GDM. On account of the complexity of raw signal attributes, a hierarchical attribute system has been established for using AHP to characterize the situation and efficiently incorporate objective and subjective factors into the decision. Correlations among the attributes are captured and reduced by fuzzy clustering and PCA. The subjective weighting necessary for the group decision-making is conducted by pairwise comparison of the relative importance of a few attribute units. The evaluation process of six GPS L1C signal modulation options has been shown as a case study. The proposed approach can mitigate the workload, difficulty,

subjectivity, and arbitrariness, and provide an effective means for comprehensive performance evaluation of satellite navigation signal options.

Some limitations in this paper and future work should be pointed out here: (1) Including more signal attributes will improve the reliability of the evaluation results, such as the receiver/payload complexity and power consumption, whereas the calculation and estimation of the attribute values are still under investigation. (2) The change of attribute values with different preconditions should also be included in the evaluation process, especially the degradations of signal performances under various imperfections of satellite payload, propagation, and receiver channels. (3) Reasonable integration of theoretical analysis, real measurements, and special test data is also worth exploring.

References

1. Xu B, Bao T (2011) Quantitative and comprehensive evaluation of qualitative index in dam safety monitoring. Adv Sci Technol Water Resour 31(5):59–63
2. Wang B (2008) Study on multi-layers and multi-objects system model for channel plan Fuzzy optimization. Dalian Maritime University
3. He J, Li Z, Wan F (2000) Method of analyzing qualitative index of comprehensive assessment for dam structure monitoring behaviour. Hydroelectric Energy
4. Liu D, Wu Z, Jia C (2005) Multi-layers and multi-objects fuzzy optimization model of main target ship. J Traffic Transp Eng
5. Meng Q, Zhao X, Zhou M (2007) Multi-attribute Fuzzy decision making for shipborne gunfire target optimum seeking. Fire Control Command Control
6. Wang HW, Shu-Lin LI, Chen N (2010) A method of solving the correlation of evaluation indices of aircraft survivability. J Air Force Eng Univ
7. Tan Y, Song W, Li T (2014) Application and research on consistency combination weights for mining method optimization by multi-objective decision. Chin J Eng 08:1115–1122
8. Ma X (2013) The research of comprehensive evaluation method for navigation signal waveforms performance. Huazhong University of Science and Technology
9. Hu X, Tang Z, Zhou H, Huang X (2009) Analysis on design principles of GPS and Galileo signal structure. Syst Eng Electron 10:2285–2293
10. Szmidt E, Kacprzyk J (2000) Distances between intuitionistic fuzzy sets. Fuzzy Sets Syst 114 (3):505–518
11. Yu J (2005) Multivariate statistical analysis and application. Sun yat-sen university press
12. Wang X (2003) A study on theories and methodologies for Fuzzy multi-objective decision making with their applications. Dalian University of Technology
13. Rao RV (2013) Decision making in the manufacturing environment using graph theory and Fuzzy multiple attribute decision making methods. Springer Series in Advanced Manufacturing. Springer, London. doi:10.1007/978-1-4471-4375-8_2
14. Liu W (2011) Study on the compatibility and interoperability of global navigation satellite system. Shanghai Jiaotong University
15. Kaplan ED, Hegarty C (2006) Understanding GPS: principles and applications. Artech House

Peak Position Detection-Based Acquisition Algorithm of Multiple Access Interference Resistance

Weina Hao and Jingyao Chen

Abstract This essay targets multiple access interference environment which is unclear to the PN sequence and investigates the reinforcing acquisition method of direct spread spectrum signal. This essay also puts forward peak position detection-based acquisition method of multi-access interference removal resistance, achieves the position information of cross-correlation interference with multi-peak characteristics through multiple detection decision, so as to remove the multi-access interference. Meanwhile, the frequency feature of the pseudo code correlation results is applied to reduce the false alarm probability through multifrequency joint detection. Both theoretical analysis and simulation results have verified the effectiveness of this method.

Keywords Direct spread signal acquisition · Multiple access interference · Peak position detection · Multiple frequency joint detection

In the space tracking and control system, the distance between responders and the ground station results in power differences of different signals, and strong signal influences the normal reception of weak signal through multi-access interference. Thus, improving multi-access interference resistance capability of signal acquisition has become an important research direction of space tracking and control technologies.

Conventional multi-access resistance algorithm removes interference through signal estimation, which needs the PN sequence information of multi-access interference. However, under some circumstances, the PN sequence of multi-access interference is unclear, so the improved acquisition strategy is needed. First of all, most research on acquisition algorithm of multi-access resistance makes

W. Hao (✉)
Academy of Opto-Electronics, Chinese Academy of Sciences,
No. 9 Deng Zhuang South Road, HaiDian District, Beijing 100094, China
e-mail: weinahao@163.Com; kramnana@sina.com

J. Chen
School of Information and Electronics, Beijing Institute of Technology,
Beijing, China

J. Sun et al. (eds.), *China Satellite Navigation Conference (CSNC) 2016 Proceedings: Volume II*, Lecture Notes in Electrical Engineering 389,
DOI 10.1007/978-981-10-0937-2_3

improvement in terms of techniques of detection decision of the correlation value. Main methods of correlation value detection include maximum detection [1], serial detection [2] and hybrid detection [3], and hybrid detection is more applicable to the FFT-based pseudo code parallel acquisition algorithm [4]. The main–sub ratio detection regards the ratio of maximum to submaximum value of the following group of frequency point results as detection decision, then compares the detection decision with detection threshold. The main–sub ratio detection has easy algorithm and CFAR characteristics, and has been widely applied in practical engineering [5]. The multi-peak detection method in reference [6] can be applied when the PN sequence of multi-access inteference is unclear. The autocorrelation peak of spread spectrum signal has only one autocorrelation main peak in a period of spreading code, while it has many cross-correlation peaks. Based on the cross-correlation feature of pseudo code, whether the current peak is a cross-correlation peak can be judged. If receivers make judgement that the current acquisition peak is a cross-correlation peak, this acquisition will be rejected. Reference [7] mentions to use the main–sub ratio as the acquisition algorithm of decision, which decreases the false alarm probability in the situation of interference resistance, yet it does not analyze the detection probability when strong multi-access signal exists.

When the PN sequence of multi-access interference is unknown, simple rejection of the cross-correlation peak mentioned in the above method reduces the false alarm probability of multi-access interference, but it does not significantly improve the detection probability. Therefore, it is necessary to investigate the acquisition algorithm when the pseudo code of multi-access interference is unclear.

1 Analysis of Algorithm Principles

The conventional multi-peak detection method makes use of different distribution features of autocorrelation peaks and cross-correlation peaks of the spreading code, detects whether cross-correlation interference exists in the process of signal acquisition, but it does not remove the cross-correlation interference. Thus, the acquisition performance is not desirable. Targeting this issue, the peak position information of cross-correlation interference can be applied to conduct interference zero setting, so as to remove multi-access interference. In addition, the peak position information can be acquired through multiple decisions by applying the multi-peak feature of cross-correlation function.

1.1 Detection Method of the Peak Position

The peak position detection-based acquisition method of multi-access interference removal needs to estimate the peak position information of cross-correlation interference when the PN sequence of multi-access interference is unclear, so as to conduct zero setting of the corresponding position of cross-correlation peaks in correlation

acquisition results. After the interference removal is completed, detection decision of peak-to-average ratio of correlation acquisition results can be performed.

This essay analyzes the algorithm performance by using the pseudo code with 0.1 ms period and 10.23 Mcps bit rate. The initial phase and generating polynomial of target pseudo code can refer to the PRN1 sequence of GPS satellites, and the initial phase and generating polynomial of interfering pseudo code can refer to the PRN2 sequence of GPS satellites.

The cross-correlation function of the PN sequence has the multi-peak feature and cross-correlation function of target pseudo code and interfering pseudo code has three possibilities, i.e., 63/1023, 1/1023, and −65/1023. The influence of cross-correlation function 1/1023 on correlation acquisition results can be omitted, so the cross-correlation function that needs to be removed is the cross-correlation peak value 63/1023 and −65/1023. Thus, the position estimation of cross-correlation peak value can be achieved by applying the correlation value as detection decision. In the FFT-based pseudo code parallel acquisition method, the Doppler frequency search applies the serial search method. Under a certain search frequency point, if the phase deviation of the corresponding pseudo code of interfering signal and target signal maintains unchanged, the peak position of cross-correlation interference in the acquisition results will be relatively fixed. Thus, in order to increase the reliability of position detection of cross-correlation peak value, it is necessary to conduct multiple detection decision. Main methods of detection decision include M/N decision, 1 + M/N decision, Tong detection, etc. This essay does not focus on multiple methods of detection decision, so the relatively simple M/N decision method is selected to conduct analysis here.

However, the correlation peak position achieved through peak position detection includes both cross-correlation peak and autocorrelation peak. If all correlation peak positions in the acquisition results are set zero, the autocorrelation peak will be lost and signal acquisition cannot be completed. Thus, when carrying out zero setting on the corresponding positions of correlation peaks in the acquisition result, the maximum of correlation peak should be kept as the acquired autocorrelation peak. Notably, maximum of the default cross-correlation peak before the multi-access interference removal represents the autocorrelation peak of target signal. Therefore, this algorithm can only achieve correct acquisition when the autocorrelation peak value is higher than cross-correlation peak value.

Based on the analysis above, the fundamentals of the acquisition method of peak position detection-based multi-access interference removal are as follows: the acquisition results of all phases in each search frequency point goes through peak position detection by using the multiple detection decision method in order, and recording all correlation peak positions. Then, among acquired correlation results under all frequency points, keeping the maximum value of the correlation peak and conducting zero setting of other correlation peaks, so as to remove the influence of cross-correlation peaks on acquisition performance. Next, performing peak–average ratio detection decision on correlation acquisition results after the zero setting of cross-correlation peaks and completing the detection period of the peak position detection-based acquisition method of multi-access interference removal.

1.2 Multiple Frequency Joint Detection Method

Based on the analysis above, the peak position detection-based multi-access interference removal algorithm can improve detection probability under fixed decision threshold. However, if only completing the detection period of the above acquisition method, the maximum of maintained correlation peaks cannot be ensured as auto-correlation peaks of target signal instead of cross-correlation peaks introduced by multi-access interference. Next, the influence of this algorithm on false alarm probability and its potential false acquisition as well as solutions will be discussed.

To inspect the influence of multi-access interference on corresponding false alarm probability and detection probability of each detection decision, the following four hypotheses should be considered:

1. H00 hypothesis: Target signal does not exist and receipt signal only contains Gaussian While Noise;
2. H01 hypothesis: Target signal does not exist and receipt signal only contains interfering signal and Gaussian While Noise;
3. H10 hypothesis: Target signal exists and receipt signal only contains target signal and Gaussian While Noise;
4. H11 hypothesis: Target signal exists and receipt signal contains target signal, interfering signal, and Gaussian While Noise;

Under the H00 hypothesis, receipt signal only contains Gaussian While Noise and peak position detection through multiple detection decision does not influence the peak value, so interference removal is not necessarily conducted and detection algorithm of correlation acquisition results will not be affected. Thus, the false alarm probability acquired by signal under the H00 hypothesis is not affected by peak position detection-based multi-access interference removal algorithm. While under the H01 hypothesis, in addition to Gaussian White Noise, receipt signal also contains interfering signal, so cross-correlation peak positions can be detected and removed through interference. As a consequence, the false alarm probability acquired under the H01 hypothesis will increase because of the application of peak position detection-based multi-access interference removal algorithm. Likewise, under the H11 hypothesis, applying the peak position detection-based multi-access interference removal might lead to false acquisition.

Under the circumstances of multi-access interference, the intermediate frequency combined signal model after receivers complete D/A switch can be represented as follows:

$$\begin{aligned} s(t) &= s_i(t) + s_j(t) + \eta(t) \\ &= A_i \cdot \mathrm{PN}_i(t-\tau_i) \cdot \cos\left[2\pi\left(f_I + f_{d,i}\right)t + \varphi_i\right] \\ &\quad + \sum_{\substack{j=1 \\ j\neq i}}^{M-1} A_j \cdot \mathrm{PN}_j\left(t-\tau_j\right) \cdot \cos\left[2\pi\left(f_I + f_{d,j}\right)t + \varphi_j\right] + \eta(t) \end{aligned} \tag{1}$$

In this formula, $s_i(t)$ is target signal; A_i represents the amplitude of target signal; $\mathrm{PN}_i(t)$ is the PN sequence of target signal; τ_j denotes the pseudo code of target signal; f_I is intermediate carrier frequency; $f_{\mathrm{d},i}$ represents Doppler frequency of target signal; φ_i is the carrier phase of target signal; $s_j(t)$ is target signal and A_j is the amplitude of interfering signal; $\mathrm{PN}_i(t)$ represents the PN sequence of interfering signal; τ_i is the pseudo code phase of interfering signal; $f_{\mathrm{d},j}$ is the Doppler frequency of interfering signal; φ_j represents the carrier phase of the interfering signal; M denotes the total number of channels of combined signals; $\eta(t)$ is Gaussian White Noise. It can be seen that the second item in formula 1 represents the multi-access interfering signal among receipt signals.

According to different frequency characteristics of autocorrelation function and cross-correlation function of pseudo code, the detection period of the above multi-access acquisition method of interference removal can be detected by means of multiple frequency joint detection method. The acquisition results under multi-access interference include autocorrelation result of target signal, the cross-correlation result of interfering signal as well as the noise item. The acquisition result $Z(\hat{\tau},\hat{f}_\mathrm{d})$ can be shown below:

$$\begin{aligned} Z\left(\hat{\tau},\hat{f}_\mathrm{d}\right) &= \frac{1}{2}A_i R_i(\Delta\tau_i)\mathrm{sinc}\left(\pi T_\mathrm{coh}\Delta f_{\mathrm{d,i}}\right)\mathrm{e}^{-j\varphi_i} \\ &\quad + \frac{1}{2T_c}A_j\mathrm{e}^{-j\varphi_j}\sum_{k=-\infty}^{+\infty}\mathrm{sinc}\left[\left(\Delta f_{\mathrm{d,j}}-\frac{k}{T_c}\right)T_\mathrm{coh}\right]\sum_{j\neq i}C_{i,j}\left(\frac{k}{T_c}\right)+n_z \end{aligned} \tag{2}$$

Next, the results of influence of Doppler frequency deviation on autocorrelation and cross-correlation are respectively analyzed from the perspective of single period coherent integration and multi-period coherent integration.

The autocorrelation part in the correlation acquisition result can be represented as follows:

$$Z_\mathrm{auto}\left(\hat{\tau},\hat{f}_\mathrm{d}\right) = \frac{1}{2}A_i R_i(\Delta\tau_i)\mathrm{sinc}\left(\pi T_\mathrm{coh}\Delta f_{\mathrm{d,i}}\right)\mathrm{e}^{-j\varphi_i} \tag{3}$$

When $\Delta\tau_i \approx 0$, $R_i(\Delta\tau_i) = 1$. The coherent integration is one pseudo code period; i.e., under the circumstance of 0.1 ms, the autocorrelation peak power when the Doppler frequency deviation is zero is regarded as the benchmark. The attenuation of autocorrelation peak power of target signals with different Doppler frequency deviations is shown in Fig. 1. It can be seen that attenuation of autocorrelation peak power conforms with characteristics of sinc function. When the Doppler frequency deviation is zero, the autocorrelation peak value is the biggest. When the Doppler frequency deviation is integral times of 10 kHz, i.e., at the zero point of sinc function, the autocorrelation peak power attenuation reaches the maximum value. As the Doppler frequency increases, the peak value of the side lobe of autocorrelation peak power function attenuates more.

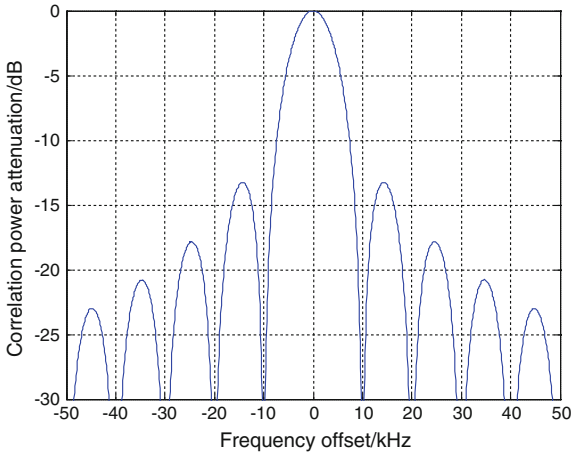

Fig. 1 Single period autocorrelation peak power attenuation of pseudo code with different Doppler frequency deviations

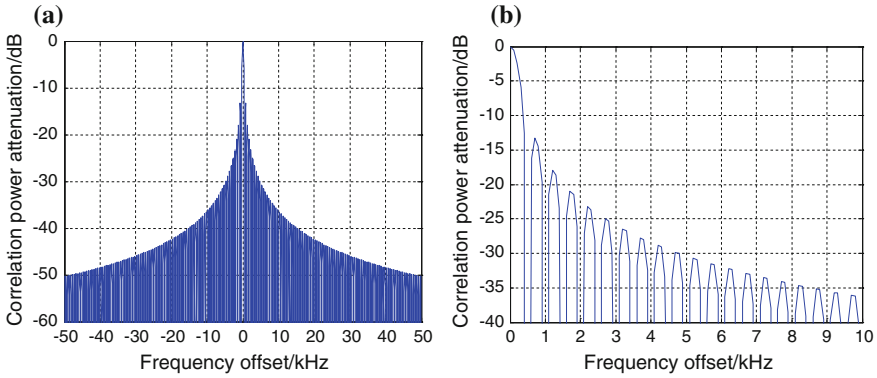

Fig. 2 Attenuation of multi-period autocorrelation peak power of pseudo codes under different Doppler frequency deviations

When the coherent integration is 20 pseudo code period (2 ms), the autocorrelation peak power when Doppler deviation is zero is regarded as the benchmark. Figure 2 shows the attenuation of autocorrelation peak power of target signal under different Doppler frequency deviations. Figure 2b is an enlarged scale of details in Fig. 2a when the Doppler frequency deviates from 0 to 10 kHz. It can be seen that under multi-period coherent integration, the attenuation of autocorrelation peak power complies with characteristics of sinc function. However, T_{coh} increases, so the position of the zero point of sinc function changes from the integral times of 10–500 Hz, but attenuation of the side lobe peak value of autocorrelation peak value still increases with the enlargement of Doppler frequency deviation.

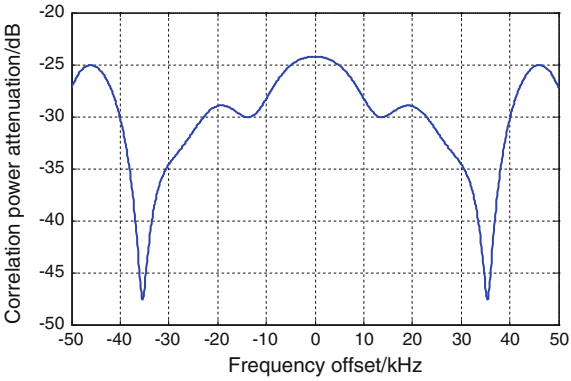

Fig. 3 Attenuation of single period cross-correlation peak value under different Doppler frequency deviations

The cross-correlation part in the acquisition result can be represented as follows [8]:

$$Z_{\text{cross}}\left(\hat{\tau},\hat{f}_{\text{d}}\right) = \frac{1}{2T_c}A_j e^{-j\varphi_j}\sum_{k=-\infty}^{+\infty}\text{sinc}\left[\left(\Delta f_{\text{d},j} - \frac{k}{T_c}\right)T_{\text{coh}}\right]\sum_{j\neq i}C_{i,j}\left(\frac{k}{T_c}\right) \quad (4)$$

When coherent integration is 1 pseudo code period (0.1 ms), for a certain fixed pseudo code phase difference, the autocorrelation peak power when Doppler frequency deviation is zero is regarded as the benchmark. Attenuation of cross-correlation peak value of target signal and interfering signal under different Doppler frequency deviations are shown in Fig. 3. It can be seen that the cross-correlation suppression capability of target signal on interfering signal is at worst around 24 dB. Theoretically, when Doppler frequency deviation is zero or integral times of the reciprocal of pseudo code period, cross-correlation interference has the strongest influence on correlation acquisition results. However, under single period coherent integration, attenuation of cross-correlation peak value of pseudo code under different Doppler frequency deviations does not significantly show the above characteristics.

When coherent integration is 20 pseudo code periods (2 ms), the autocorrelation peak power when Doppler deviation is zero is regarded as the benchmark. Figure 4 shows attenuation of cross-correlation peak power of target signal and interfering signal under different Doppler frequency deviations. Figure 4b is an enlarged scale of details in Fig. 4a when the Doppler frequency deviates from 0 to 10 kHz. It can be seen that under multi-period coherent integration, the zero point of sinc function is situated at the integral times of 500 Hz. Distinct from attenuation of autocorrelation peak power, attenuation of pseudo code cross-correlation peak value varies periodically with multiple frequency deviations. When Doppler frequency deviation is 0 or the integral times of 10 kHz, the peak power of pseudo code cross-correlation reaches the maximum value.

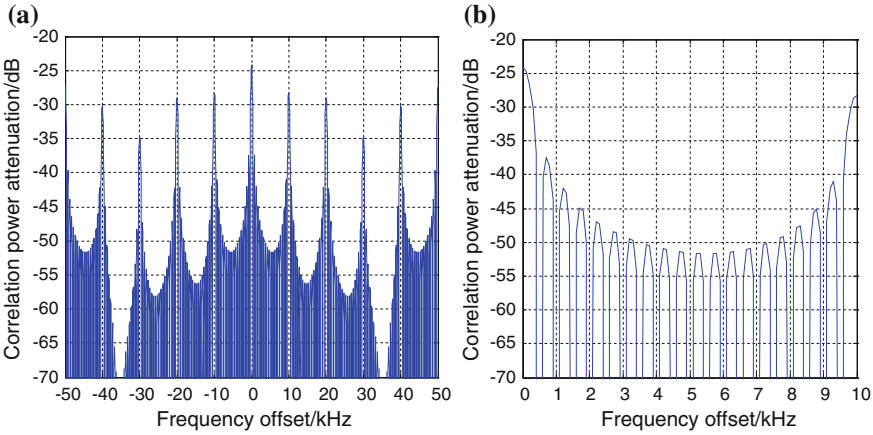

Fig. 4 Attenuation of multi-period cross-correlation peak power of pseudo code under different Doppler frequency deviations

Thus, when coherent integration has multiple pseudo code periods, if Doppler frequency deviation is the integral times of 10 kHz, attenuation of autocorrelation peak value is the most distinct, while attenuation of the peak value of cross-correlation is almost the same. Therefore, this feature can be used to distinguish autocorrelation peak and cross-correlation peak. In order to avoid the acquisition method of peak value position detection-based multi-access interference removal incorrectly treating the cross-correlation peaks of multi-access interfering signal as autocorrelation peaks of target signal, correlation results of all frequency points under corresponding pseudo code of correlation peaks can go through multifrequency joint detection. If the result complies with frequency characteristics of pseudo code autocorrelation function, this correlation peak is the autocorrelation peak and the corresponding Doppler frequency in the unit cell and the pseudo code phase represents the result of this acquisition. Otherwise, the correlation peak is the cross-correlation peak of interfering signal and the current acquisition result should be rejected.

Based on the analysis above, the design thought of multifrequency joint detection-based acquisition algorithm is as follows: first of all, under each frequency point, using the multi-peak feature of pseudo code cross-correlation function to detect the position information of cross-correlation interference and remove cross-correlation peak interference except the maximum value. Then, detecting the acquisition result and applying different frequency features of autocorrelation peaks and cross-correlation peaks to conduct multifrequency joint detection on the current acquisition result. If it is an autocorrelation peak, the acquisition result can be output; otherwise the acquisition of target signal is unsuccessful.

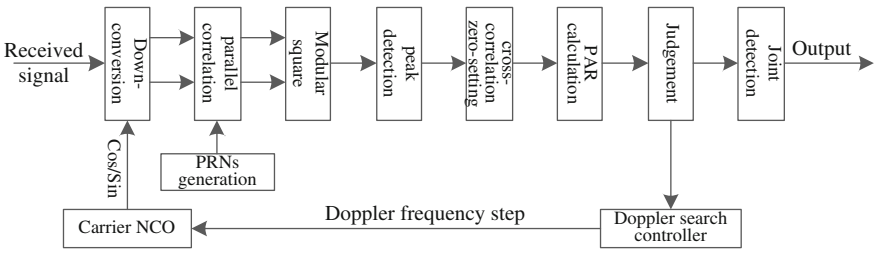

Fig. 5 Process of peak position detection-based acquisition method of multi-access interference removal

1.3 Summary of the Algorithm Process

The process of the peak position detection-based acquisition method of multi-access interference removal is shown in Fig. 5.

Detailed procedures of the process are shown below:

1. When acquisition starts up, the carrier NCO module receives the Doppler frequency word, the two-path orthogonal local carrier signal is generated and output to the down-conversion module.
2. The down-conversion module receives local carrier signal and input signal, and completes the Doppler frequency liftoff through orthogonal down-conversion algorithm, achieving path *I* (in-phase) baseband signal and path *Q* (orthogonal) baseband signal;
3. Pseudo code generator produces a pseudo code period of target signal with the length of one pseudo code period and output to parallel correlation modules;
4. In parallel correlation modules, the result of down-conversion and the local PN sequence produced by the local pseudo code generator go through parallel correlation, then output the correlation result;
5. Modular square module receives the parallel correlation result and conduct square algorithm after modular multiplication algorithm, then output the modular square result to the peak position detection module.
6. The peak position detection module conduct multiple correlation detection decision on all correlation results and output the acquisition result as well as the correlation peak result information to the cross-correlation peak zero-setting module;
7. Based on received information of correlation peak position, cross-correlation zero-setting module performs zero setting on module square value where correlation peaks appear except the maximum value in the result. Then, output the zero-setting module square result to the peak–average ratio so as to calculate modules;
8. Finding out the peak position from the correlation result output by correlation peak zero-setting module calculated through the peak–average ratio. Using data except the peak value to calculate the average noise value and output the

peak–average ratio (PAR) calculated by peak-to-noise average value to the decision module;

9. Detecting the peak–average ratio received by the decision module to calculate the peak–average ratio, and conducting detection decision with the threshold; if the peak–average ratio is smaller than the threshold, it means no signal has been acquired, and the Doppler search and control module will be notified; if the peak–average ratio is bigger than threshold, the peak–average ratio and the acquisition phase will be output to the Doppler search and control module;
10. In the Doppler search and control module, if the detection decision module does not exceed the threshold, the output Doppler frequency word will be updated, then enters procedure 1; if the detection decision module exceeds threshold, this peak–average ratio will be compared against the maximum peak–average ratio (the initial value is 0) stored previously. If it is larger than stored maximum peak–average ratio, maximum peak–average ratio, the acquisition phase and the current Doppler frequency word will be updated, then enters procedure 1;
    Under the control of the Doppler search and control module, repeating procedures 1 to 10 till completing searching all Doppler frequency words;
11. After the Doppler search and control module output all Doppler frequency words, if stored maximum peak–average ratio maintains 0, it means the initial acquisition is unsuccessful, then back to procedure 1; if stored maximum peak–average ratio is not 0, it means the initial acquisition is successful, stored acquisition phase and the acquisition results under corresponding multiple Doppler frequency points will be output to multifrequency joint detection modules;
12. Multifrequency joint detection modules conduct detection decision according to received pseudo code phase and its corresponding correlation results. If the correlation peak module value is significantly higher than other frequency points in a certain frequency point, this acquisition is successful, and this frequency point represents acquired Doppler frequency. The received pseudo code phase is acquired pseudo code phase and the acquisition result can be output; otherwise, the acquisition is unsuccessful, then back to procedure 1.

2 Verification of Algorithm Simulation

This section conducts simulation verification on the peak position detection-based acquisition method of multi-access interference removal through Monte Carlo simulation. This section also compares the conventional acquisition method with the peak position detection-based acquisition of multi-access interference removal (the acquisition method used in this essay), and the parametric setting is shown in Table 1.

Table 1 Simulation parametric setting

Parameter	Value	Unit
PN sequence of target signal	PRN1	–
PN sequence of interfering signal	PRN2	–
Speed of pseudo code	10.23	MHz
Frequency of intermediate frequency	15	MHz
Coherent integration time	0.5	Ms
Doppler search step	1	kHz

2.1 Simulation of Pre-detection Peak–Average Ratio

In order to conveniently observe the effect of the peak position detection-based acquisition of multi-access interference removal, simulation of acquisition correlation result of noise-free signal of interfering signal only in path 1 and pre-detection peak–average ratio is conducted.

1. No Doppler frequency deviation exists between multi-access interfering signal and target signal.

Figures 6 and 7 respectively represent the correlation results when no Doppler frequency deviation exists between multi-access interfering signal and target signal, and the two-dimensional correlation results acquired by noise-free signal before and after interference is removed. Applying the peak position detection-based acquisition of multi-access interference removal can remove certain cross-correlation interference and improve the pre-detection peak–average ratio. Under search frequency points with integral times of 10 kHz of the Doppler frequency difference of multi-access interfering signal, the influence of multi-access interfering signal on the acquisition result is the biggest and the correlation peak is kept after removing interference, among which the autocorrelation peak value of target frequency point is the largest.

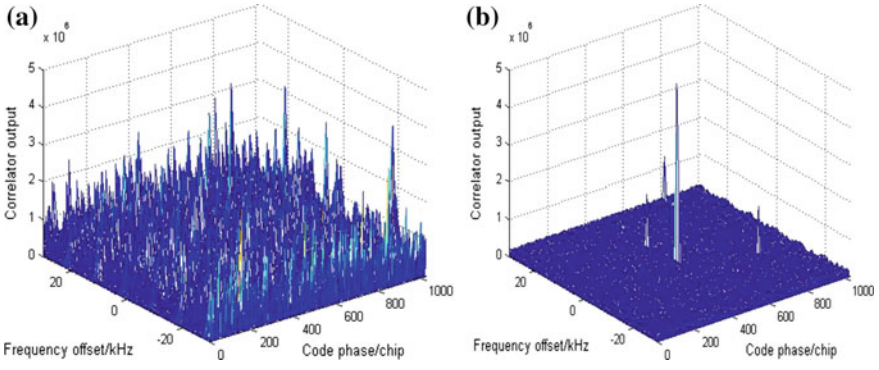

Fig. 6 Acquisition correlation results before and after noise-free signal interference removal (no frequency difference). **a** Before interference removal. **b** After interference removal

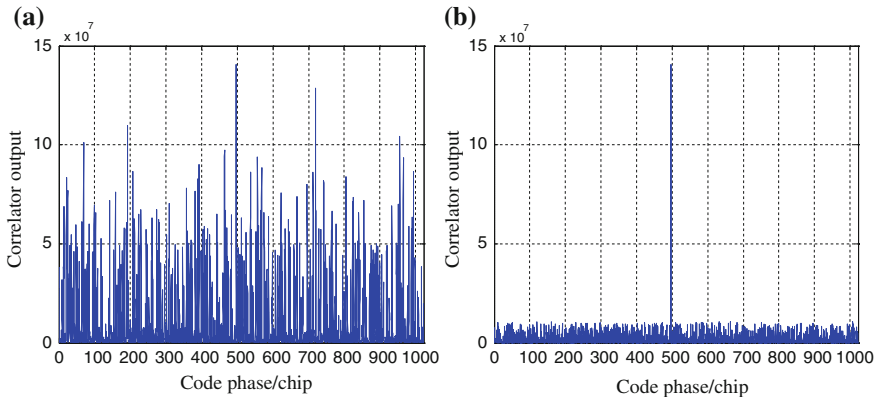

Fig. 7 Acquisition correlation result of signal frequency points before and after noise-free signal removal (no frequency difference). **a** Before interference removal. **b** After interference removal

2. Doppler frequency deviation exists between multi-access interfering signal and target signal.

Figures 8 and 9 respectively represent the acquisition two-dimensional search correlation results of noise-free signal before and after interference removal and correlation result of target frequency points when the Doppler frequency difference between multi-access interfering signal and target signal is 10 kHz. After applying the peak position detection-based acquisition of multi-access interference removal, certain cross-correlation interference can be removed under the circumstances of Doppler frequency difference. Pre-detection signal-to-noise ratio is improved, but certain cross-correlation peak is still maintained on nontarget frequency points.

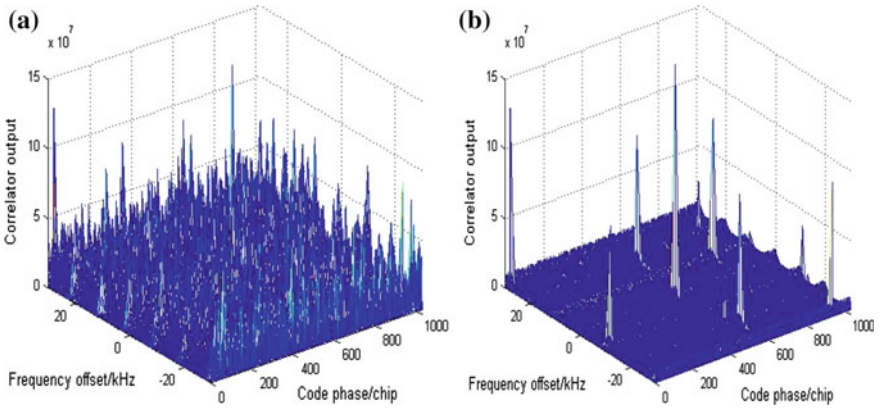

Fig. 8 Acquisition correlation results before and after removing the noise-free signal interference. **a** Before interference removal. **b** After interference removal

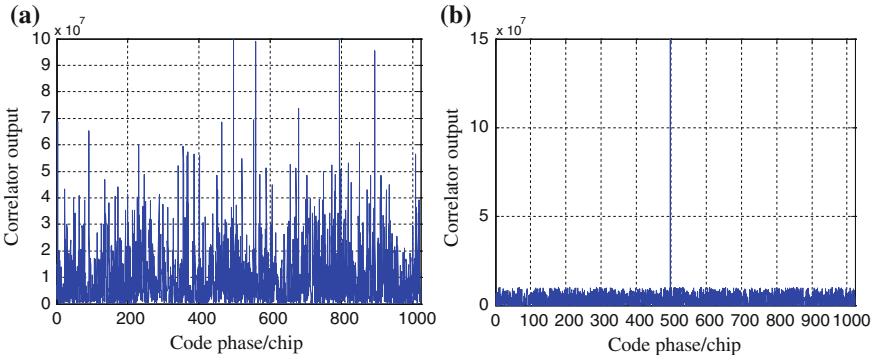

Fig. 9 Acquisition correlation results of target frequency points before and after removing the noise-free signal interference. **a** Before interference removal. **b** After interference removal

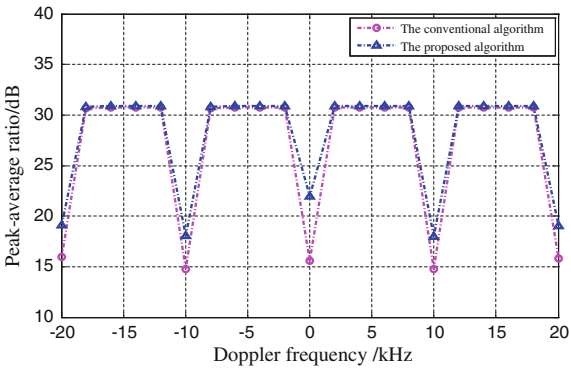

Fig. 10 Comparison of detection peak–average ratio before and after interference removal under different Doppler frequency deviations

When Doppler frequency deviation exists between multi-access interfering signal and target signal, the influence of cross-correlation interference on acquisition correlation results under different Doppler frequency deviations is distinct. Figure 10 shows the comparison between pre-detection peak–average ratio before and after interference removal under different Doppler frequency deviation. When the Doppler frequency deviation is 0 or the integral times of 10 kHz, cross-correlation interference has more significant influence on the acquisition result. The pre-detection peak–average ratio of conventional detection method is relatively low and the pre-detection peak–average ratio after interference removal is significantly increased, so the detection probability is improved. When applying the acquisition method investigated in this essay, the pre-detection peak–average ratio is the best when the Doppler frequency deviation is 0 and peak–average ratio increases about 7 dB. When the Doppler frequency deviation is the integral times of 10 kHz, the effect of interference removal is decreased. However, compared with the unprocessed situation, the peak–average ratio still increases above 3 dB. Under other Doppler frequency deviations, cross-correlation peaks are relatively small and the

pre-detection peak–average ratio is high, and interference removal is not necessary. Thus, the application of the algorithm of this essay does not influence the pre-detection peak–average ratio.

Based on the analysis above, applying the peak position detection-based acquisition method of multi-access interference removal can effectively remove interference and increase pre-detection peak–average ratio. However, when Doppler frequency difference exists between target signal and multi-access interfering signal and the difference is the integral times of 10 kHz, the effect of interference removal has certain decline.

2.2 *Simulation of False Alarm Probability*

In order to ensure the acquisition method in this essay conforms to the requirements of false alarm probability, the false alarm probability in receipt signal which only includes interfering signal is conducted simulation verification. Figure 11 shows the false alarm probability comparison of the peak position detection-based acquisition method of multi-access interference removal and the conventional acquisition method under different interfering signal SNR. With the application of the algorithm in this essay, when the multi-access interfering signal SNR is relatively low, the false alarm probability is a bit higher than that of conventional acquisition method. This is because the frequency feature of cross-correlation peaks is influenced by noise so that the effect of reducing false alarm is compromised. As the signal SNR of multi-access interference increases, the constant false alarm probability in the acquisition of this essay gradually declines and conforms to the requirements of constant false alarm detection. Thus, it is still necessary to compare the detection probability of conventional acquisition method and the method of this essay.

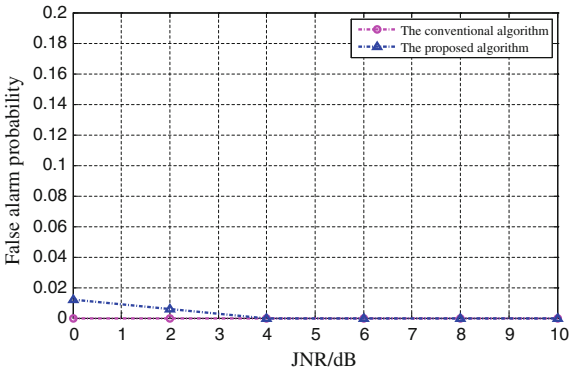

Fig. 11 False alarm probability under different interfering signal SNR

2.3 Simulation of Detection Probability

This section focuses on analyzing the acquisition performance of the peak position detection-based method of multi-access interference removal under the Gaussian channel. Two situations are considered: no Dopper frequency deviation exists between multi-access interfering signal and target signal; 10 kHz Doppler frequency deviation exists between multi-access interfering signal and target signal. The detection probability of the conventional acquisition method and the method in this essay is compared.

1. No Doppler frequency deviation exists between multi-access interfering signal and target signal.

Figure 12 compares the detection probability of the conventional acquisition method and the method of this essay under different target signal SNR when multi-access interfering signal SNR is 0 dB and no Doppler frequency deviation exists between multi-access interfering signal and target signal.

In the conventional method, when the target signal SNR is higher than −15 dB, the detection probability can achieve 90 % above; while the target signal SNR of this essay is higher than −17 dB, the detection probability can achieve 90 % above. Thus the acquisition sensitivity increases about 2 dB.

Figure 12 shows the detection probability comparison of the acquisition method of multi-access interference removal of the conventional method and the method of this essay under different SINR when the target signal SNR is −15 dB and no Doppler frequency deviation exists between the multi-access interfering signal and target signal (Fig. 13).

When the detection probability is above 90 %, the multi-access interference resistant capability of conventional acquisition method can achieve 15 dB, while that of this essay achieves around 17 dB. Thus the multi-access interference resistant capability improves about 2 dB.

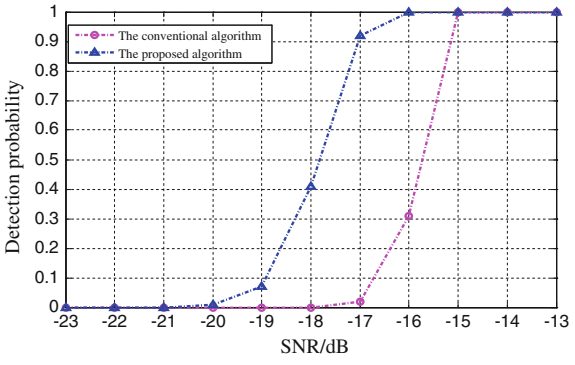

Fig. 12 Detection probability of algorithm under different target signal SNR (no frequency difference)

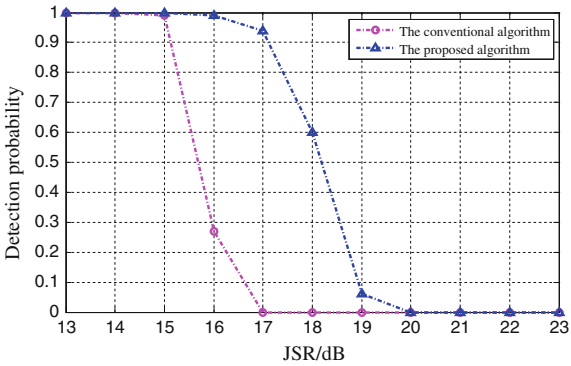

Fig. 13 Detection probability of algorithm under different SINR (no frequency difference)

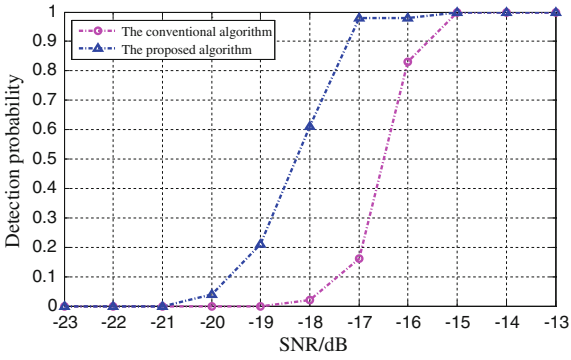

Fig. 14 Detection probability of algorithm under different target signal SNR (10 kHz frequency difference)

2. 10 kHz Doppler frequency deviation exists between multi-access interfering signal and target signal.

Figure 14 compares the detection probability of the conventional acquisition method and the method of this essay under different target signal SNR when multi-access interfering signal SNR is 0 dB and 10 kHz Doppler frequency deviation exists between multi-access interfering signal and target signal.

In the conventional method, when the target signal SNR is higher than −15.5 dB, the detection probability can achieve 90 % above; while the target signal SNR of this essay is higher than −17 dB, the detection probability can achieve 90 % above. Thus the acquisition sensitivity increases about 1.5 dB.

Figure 15 shows the detection probability comparison of the acquisition method of multi-access interference removal of the conventional method and the method of this essay under different SINR when the target signal SNR is −15 dB and 10 kHz Doppler frequency deviation exists between the multi-access interfering signal and target signal.

When the detection probability is above 90 %, the multi-access interference resistant capability of conventional acquisition method can achieve 16 dB, while

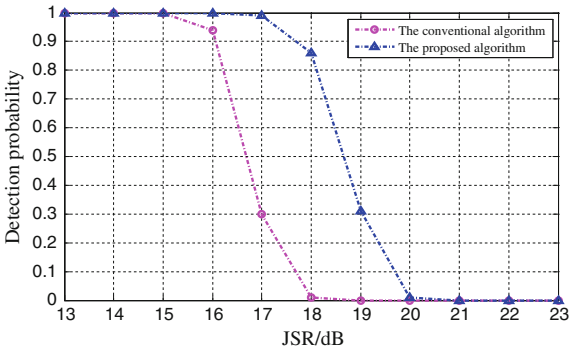

Fig. 15 Detection probability of algorithm under different SINR (10 kHz frequency difference)

that of this essay achieves around 17.5 dB. Thus the multi-access interference resistant capability improves about 1.5 dB.

Based on the analysis above, simultaneously applying the peak position detection-based acquisition method of multi-access interference removal can effectively achieve interference removal under the Gaussian channel, so as to improve the detection probability of signal acquisition. When the interfering signal SNR is fixed, applying this method can enhance the acquisition sensitivity; while when the target signal SNR is fixed, the application of this method can improve the multi-access interference resistance capability of acquisition. In addition, when 10 kHz Doppler frequency difference exists between multi-access interference signal and target signal, the multi-access interference resistance capability of this algorithm has certain decline compared with when no Doppler frequency difference exists.

3 Conclusion

This essay investigates the acquisition technique of multi-access interference removal when the PN sequence of interfering signal is unclear. Based on the design thought of applying cross-correlation interference position to remove interference and the multi-peak feature of pseudo code cross-correlation function, this essay put forward the acquisition method of multi-access interference removal based on peak position detection and illustrates the process of algorithm in detail. In terms of the increased acquisition false alarm probability and the potential false acquisition issue, this essay reduces the false alarm probability through multifrequency joint detection to complete the detection period of acquisition. This algorithm can improve multi-access interference resistance capability under different Doppler frequency deviations.

References

1. Corazza GE (1996) On the MAX/TC criterion for code acquisition and its application to DS-SSMA systems. IEEE Trans Commun 44(9):1173–1182
2. Polydoros A, Weber C (1984) A unified approach to serial search spread-spectrum code acquisition-part I: general theory. IEEE Trans Commun 32(5):542–549
3. Stirling-Gallacher RA, Hulbert AP, Povey GJ (1996) A fast acquisition technique for a direct sequence spread spectrum signal in the presence of a large Doppler shift. In: Proceedings of ISSSTA, vol 1, pp 156–160
4. Smidt J (2011) Statistical characterization of a constant false alarm detector for GNSS signals. In: International conference on localization and GNSS (ICL-GNSS), pp 98–103
5. Geiger BC, Soudan M, Vogel C (2010) On the detection probability of parallel code phase on the detection probability of parallel code phase. In: IEEE 21st international symposium on personal indoor and mobile radio communications, pp 865–870
6. Zheng B, Lachapelle G (2005) GPS software receiver enhancements for indoor use. In: Proceedings of ION GNSS, pp 1139–1140
7. Wang YQ, Wu SL (2011) New acquisition decision algorithm for multiple access interference suppression in DSSS system. J Syst Eng Electr 22(1):157–163
8. Qaisar SU, Dempster AG (2011) Cross-correlation performance assessment of global positioning system (GPS) L1 and L2 civil codes for signal acquisition. IET Radar Sonar Navig (2011)

Overall Performance Comparison of Three Dual-Frequency Constant Envelop Modulation Schemes for GNSS

Yang Gao, Chunxia Li, Li Fu and Henglin Chu

Abstract In Global Navigation Satellite Systems, dual-frequency constant envelop modulation scheme includes ACE-BOC, TD-AltBOC, and AltBOC. The three modulation schemes have pros and cons on single item evaluation index such as ranging precision, navigation message demodulation performance, et al., which cause difficulties for the comparison and final chosen. In this article, a method to evaluate the overall performance of navigation signals is proposed. This method takes the minimal signal power that satisfies some positioning precision as the evaluation index, which requires enough precise ranging as well as enough good navigation message demodulation at the same time, thus can reflect the overall performance of the signal in actual using. The overall performance of the three modulation schemes was compared by bed testing under conditions that the signal used the mainstream bit rate and channel encoding method. The bed testing results show that, for 3-D positioning precision better than 10 m, the ACE-BOC need the minimal signal power, 0.5–2.5 dB lower than that for TD-AltBOC and AltBOC, thus the ACE-BOC has the best overall performance of the three schemes.

Keywords Global navigation satellite systems · Dual-frequency constant envelop modulation scheme · Signal overall performance · Minimal signal power

1 Introduction

Dual-frequency constant envelop modulation is one important technique for GNSS signal design, which can modulate two navigation signals to the upper side band and the lower side band of a wide band signal to provide individual service as well as combined service, and usually used for Aeronautical Radio Navigation Service signal design. Currently, dual-frequency constant envelop modulation schemes include ACE-BOC [1–5], TD-AltBOC [6], and AltBOC [7] et al. Signal performance

Y. Gao (✉) · C. Li · L. Fu · H. Chu
Beijing Navigation Center, Beijing 100094, China
e-mail: bikong_001@aliyun.com; bikong_001@yahoo.com.cn

J. Sun et al. (eds.), *China Satellite Navigation Conference (CSNC) 2016 Proceedings: Volume II*, Lecture Notes in Electrical Engineering 389,
DOI 10.1007/978-981-10-0937-2_4

is one important reference for the final chosen of the three schemes, thus, signal designers and other researchers have made a lot of comparison [8]. However, this comparison mostly focused on single item evaluation index like ranging precision, demodulation performance, multipath performance, and compatibility. While under the premise of limited power and bandwidth, those items may compete with each other, for instance, the more signal power assigned to the pilot branch, the better ranging but the worse demodulation performance, and the more signal power assigned to the data branch, the better demodulation but the worse ranging performance, which may confuse the comparison and make the choice more difficult. Thus, a method to compare the overall performance instead of single item performance is needed. This paper suggests a method to compare the overall performance for the three modulation schemes. By considering the main differences among the three schemes, this method takes the minimal signal power that meets some positioning accuracy as the evaluation index, which requires signal ranging and demodulation performance good enough at the same time, thus can reflect the signal overall performance in actual using. By using this evaluating method, the three schemes performance was compared by bed testing. The bed testing took the mainstream bit rate and channel encoding method as the signal design conditions, and used navigation signal simulator and five kinds of receivers to got the minimal signal power (which is "acquiring threshold" and "tracking threshold" here) for each schemes. The result shows that, ACE-BOC scheme has the best overall performance, AltBOC, and TD-AltBOC have the similar overall performance.

2 Schemes and Differences

2.1 Modulation Schemes

To meet the dual-frequency Aeronautical Radio Navigation Service, GNSS needs to provide two signals in a wide band. Navigation satellites usually emit the two signals coherently, specifically, the satellite emits a wideband constant envelope signal, whose lower side band and upper side band provide the two signal service, and the two can also be received as one signal to get more precise service. Aeronautical Radio Navigation Service band is 1151–1215 MHz [8], which is named E5 in Galileo, L5 in GPS and B2 in BDS. Here, we take the name in BDS as reference, thus the lower side band signal is denoted as B2a, and the upper side band signal is denoted as B2b.

ACE-BOC, TD-AltBOC and AltBOC can all meet the previous mentioned Aeronautical Radio Navigation Service signal requirement. They all use 15.345 MHz carrier to modulate the B2a and B2b to the lower side band and the upper side band, the B2a and B2b signals both consists of data branch and pilot branch, and all branches use 10.23 Mbps pseudo noise (PN) code. The main

differences of the three schemes are in the multiplexing method and power assignment method of data and pilot branches.

TD-AltBOC uses time division multiplexing method, emits the pilot PN code chip and data PN code chip in even and odd time slots, respectively, thus the power ratio of pilot and data branches is 1:1 [6].

AltBOC uses phase division multiplexing method, modulates the data PN code and the pilot PN code on I and Q, respectively, and limited by the constant envelope constraint, the power ratio of pilot and data branches is 1:1 [7].

ACE-BOC also uses phase division multiplexing method, but different from AltBOC, it can assign the pilot and data power ratio arbitrary even under the constant envelop constraint. The concrete ACE-BOC scheme power ratio of pilot and data branches is 3:1 [1–5].

2.2 Performance Differences

There are many items for navigation signal evaluation, such as ranging precision, multipath performance, compatibility, demodulation performance etc. While for the three schemes focused in the paper, the compatibility and multipath performance may the same as they have the similar PN code rate, bandwidth and spectrum. The main difference is the power assignment way, comparing with AltBOC and TD-AltBOC, ACE-BOC assigns more power to pilot branches (the same with the newest GPS L1C signal [9, 10]), so ACE-BOC provides better potentials on tracking and ranging (1.76 dB better in theory), but worse ability on demodulation (3.0 dB worse in theory).

3 Overall Performance Evaluation Method

3.1 Evaluation Index Design

As introduced previously, the performance differences of ACE-BOC, TD-AltBOC and AltBOC are mainly caused by the power assignment ways. ACE-BOC provides way to assign the power ratio arbitrary, which brings more choices for signal design. While limited by the total signal power, different power assignment is essentially the competition of ranging performance and demodulation performance, so individually comparing the two performances is not important anymore, instead, in one assignment way, the signal overall performance in practical use is more significant.

For navigation signal, the overall performance consists of two parts: to provide enough accuracy ranging (or keeping receiver tracking), to provide right data demodulation and these two must be satisfied at the same time. For the whole navigation satellite system, to meet the overall performance, the lower power one

signal schemes needs, the easier the scheme is for the satellite implement; For the navigation users, to meet the overall performance, the lower power one signal scheme needs, the easier the scheme is for the receiver use. Apparently, for both the system and the users, the minimal signal power to meet the signal use is a key factor, so it can be taken as the evaluation index to compare the three schemes.

3.2 Evaluation Index Definition

Based on the previous analysis and the way that navigation receiver uses signals, two kinds of evaluation indexes are defined here, i.e., **acquisitioning threshold** and **tracking threshold**. The acquisitioning threshold is defined as the minimal signal power one signal scheme needed to make the receiver output specified accuracy positioning results in specified time in cold start condition. The tracking threshold is defined as the minimal signal power one signal scheme needed to keep the receiver output specified accuracy positioning results in specified time.

Here, the acquisitioning threshold reflects the difficulties receivers have to turn to synchronized state from unsynchronized state when using one signal scheme. The tracking threshold reflects the difficulties receivers have to keep the synchronized state when using one signal scheme.

3.3 Evaluation Index Analyzing Method

Signal performance can be analyzed in many ways such as theory, simulation and actual testing. Theory analysis and simulation method are applicable to the analysis of the single performance like ranging accuracy and demodulation performance, and are often under the assumption of single signal processing steady stage. While, for comparing the overall performance, the proposed evaluation index involves several signal processing stages, and including many transient stages, thus, the theory and simulation is not suitable anymore. The proposed evaluation index will be analyzed by testing ways.

4 Overall Performance Test and Comparison

4.1 Test Conditions

Some conditions must be determined before the acquisition threshold and tracking threshold test, because the thresholds relates to several factors besides the power assignment, those factors includes data bit rate, channel encoding method, receiver RF device and receiver algorithms.